

1 **Pre-existing antibodies targeting a dominant linear antibody epitope on**  
2 **SARS-CoV-2 S2 cross-reacted with commensal gut bacteria and shaped**  
3 **immune responses elicited by a candidate vaccine**

4 Liqiu Jia<sup>1, §</sup>, Shufeng Weng<sup>2, §</sup>, Jing Wu<sup>1, §</sup>, Xiangxiang Tian<sup>3, 4</sup>, Yifan Zhang<sup>3, 4</sup>,  
5 Xuyang Wang<sup>1</sup>, Jing Wang<sup>3, 5</sup>, Dongmei Yan<sup>5</sup>, Wanhai Wang<sup>4</sup>, Zhaoqin Zhu<sup>3, #</sup>,  
6 Chao Qiu<sup>6, #</sup>, Wenhong Zhang<sup>1, 2, 7, 8, #</sup>, Ying Xu<sup>2, #</sup>, Yanmin Wan<sup>1, 2, 9, #</sup>

7

8 <sup>1</sup> Department of Infectious Diseases, National Medical Center for Infectious Diseases,  
9 Shanghai Key Laboratory of Infectious Diseases and Biosafety Emergency Response,  
10 Huashan Hospital, Shanghai Medical College, Fudan University, Shanghai, China;

11 <sup>2</sup> State Key Laboratory of Genetic Engineering, Institute of Genetics, School of Life  
12 Science, Fudan University, Shanghai, China;

13 <sup>3</sup> Department of laboratory medicine, Shanghai Public Health Clinical Center, Shanghai,  
14 China;

15 <sup>4</sup> Clinical Laboratory, The First Affiliated Hospital of Zhengzhou University, Key Laboratory  
16 of Laboratory Medicine of Henan Province, Zhengzhou, Henan, P.R. China;

17 <sup>5</sup> Department of Immunology, School of Basic Medical, Jiamusi University, Jiamusi,  
18 Heilongjiang Province, China;

19 <sup>6</sup> Institutes of biomedical sciences & Shanghai Key Laboratory of Medical Epigenetics,  
20 Fudan University, Shanghai, China;

21 <sup>7</sup> National Clinical Research Center for Aging and Medicine, Huashan Hospital, Shanghai  
22 Medical College, Fudan University, Shanghai, China;

23 <sup>8</sup> Key Laboratory of Medical Molecular Virology (MOE/MOH) and Institutes of Biomedical  
24 Sciences, Shanghai Medical College, Fudan University, Shanghai, China.

25 <sup>9</sup> Department of radiology, Shanghai Public Health Clinical Center, Shanghai, China

26 § These authors contribute equally to this work.

27 # Correspondence should be addressed to: Zhaoqin Zhu, zhaqinzh@163.com; Chao  
28 Qiu, qiuchao@fudan.edu.cn; Wenhong Zhang, zhangwenhong@fudan.edu.cn; Ying Xu,  
29 yingxu2520@fudan.edu.cn; Yanmin Wan, yanmin\_wan@fudan.edu.cn

30

31 **Running title:** Antibody cross-reactivity between SARS-CoV-2 and gut  
32 microbiota

33 **Word count:** Abstract, 203; main text, 5746

NOTE: This preprint reports new research that has not been certified by peer review and should not be used to guide clinical practice.

34 **Abstract**

35 Pre-existing SARS-CoV-2 cross-reactive antibodies have been detected in  
36 both unexposed human and animals. However, the origins of these  
37 cross-reactive antibodies and their potential impacts on vaccine efficacy have  
38 not been completely clarified. In this study, we demonstrated that the S2  
39 subunit was the predominant target of the pre-existing SARS-CoV-2 spike  
40 protein cross-reactive antibodies in both healthy human and naïve SPF mice.  
41 Through linear epitope mapping, we identified a dominant antibody epitope on  
42 the connector domain of S2 (aa1145-aa1162), which could be recognized by  
43 antibodies pre-existed in unexposed human and mice. Six monoclonal  
44 antibodies against this linear epitope were isolated from naïve SPF mice and  
45 were proved to cross-react with commensal gut bacteria collected from both  
46 human and mouse. Via immunizing mice with a candidate DNA vaccine  
47 encoding the full length of SARS-CoV-2 spike protein, we further  
48 demonstrated that high levels of pre-existing S2 cross-reactive antibodies did  
49 not impair the immunogenicity of the DNA vaccine. On the contrary, mice with  
50 high levels of pre-existing antibodies mounted stronger S2 specific binding  
51 antibody responses compared to mice with low levels of pre-existing  
52 antibodies. In addition, S1 specific T cell and binding antibody responses also  
53 tended to be enhanced in mice with high levels of pre-existing antibodies.

54

55 **Key words:** Cross-reactive antibody, SARS-CoV-2, Spike protein, commensal  
56 gut bacteria, vaccine immunogenicity

57

58

59

60

61

62

63

64

## 65 Introduction

66 Antibodies are vital components of the immune system that mediate protection  
67 against infections (1). When confronting infections, the actual role of  
68 pre-existing antibody depends on the following features (2): High titers of  
69 broadly neutralizing antibodies can protect the host against infection. While,  
70 when the pre-existing antibodies are non-neutralizing or with only a narrow  
71 neutralizing spectrum, hosts may not be sterilely protected or only be protected  
72 against specific serotypes of viruses. In addition to defending hosts against  
73 infections, pre-existing antibodies can also impact host immune responses  
74 upon infection or vaccination (3-5), which is best exemplified by the  
75 observations showing that pre-existing antibodies shaped the recall immune  
76 responses against influenza (6, 7).

77 For most occasions, pre-existing antibodies in adults derive from previous  
78 infection or vaccination except some “naturally” produced, poly-reactive  
79 antibodies (2, 8). When encountering a newly emerged or mutated virus,  
80 cross-reactive antibodies induced by previously occurred, phylogenetically  
81 closely related viruses constitute the main body of the pre-existing  
82 cross-reactive antibodies. The effect of this kind of pre-existing antibodies has  
83 been extensively investigated especially for infections of influenza (3, 7, 9) and  
84 flaviviruses (10-12). Of note, previous infection by phylogenetically similar  
85 viruses is not the sole source of pre-existing cross-reactive antibodies, as it  
86 has been clearly clarified that pre-existing antibodies against HIV-1 gp41 may  
87 stem from exposures to certain commensal gut bacteria (13-15). Besides,  
88 autoimmune diseases caused by cross-reactivities between microbial and  
89 self-antigens also implied that commensal gut bacteria represent important  
90 sources of cross-reactive antibodies (16-19).

91 Pre-existing antibodies against SARS-CoV-2 have also been observed in  
92 uninfected healthy individuals, which are speculated to be engendered by  
93 previous exposures to human common cold coronaviruses (20-26) or  
94 SARS-CoV (27-29). Meanwhile, sequence analyses (30) and a clinical  
95 observation (31) suggest that pre-existing SARS-CoV-2 antibodies might be  
96 engendered by common human pathogens and childhood vaccination.  
97 Although these two explanations are not mutually exclusive, they both need  
98 more experimental evidence to support.

99 In this study, we found that higher levels of SARS-CoV-2 S2 protein specific

100 antibodies existed in both healthy human and naïve SPF mice. To track the  
101 potential origins of these pre-existing cross-reactive antibodies, we mapped  
102 and located a dominant linear antibody epitope on S2, which could be  
103 recognized by pre-existing antibodies from both healthy human and naïve SPF  
104 mice. Monoclonal antibodies against this linear epitope were isolated from  
105 naïve SPF mice and proved to cross-react with commensal gut bacteria  
106 collected from both healthy human and naïve SPF mouse. Moreover, despite  
107 having been discussed iteratively (32, 33), the influences of pre-existing  
108 cross-reactive immunities on COVID-19 responses have not been clarified.  
109 Here we showed that high levels of pre-existing antibodies did not impair the  
110 immunogenicity of a candidate DNA vaccine encoding SARS-CoV-2 spike  
111 protein. On the contrary, mice with high levels of pre-existing antibodies  
112 mounted stronger S2 specific binding antibody responses compared with mice  
113 with low levels of pre-existing antibodies after immunization with a candidate  
114 DNA vaccine. Meanwhile, S1 specific T cell and binding antibody responses  
115 also tended to be stronger in mice with high levels of pre-existing antibodies,  
116 although no statistical significance was reached.

117

## 118 **Materials and methods**

### 119 **Ethics statement**

120 All experiments and methods were performed in accordance with relevant  
121 guidelines and regulations. Experiments using mice and samples of healthy  
122 human were approved by the Research Ethics Review Committee of the  
123 Shanghai Public Health Clinical Center Affiliated to Fudan University.

124

### 125 **Plasma samples of healthy human**

126 Two batches of plasma samples were collected from healthy individuals at the  
127 health screening clinic of Shanghai Public Health Clinical Center. A concurrent  
128 batch was collected in December 2020. All the 95 individuals enrolled in this  
129 batch reported no epidemiological link with confirmed COVID-19 patients and  
130 were confirmed to be free from any chronic or acute disease. Viral RNA tests  
131 confirmed that all individuals in this batch were free from SARS-CoV-2  
132 infection. In addition, a historical batch of 78 plasma samples from healthy  
133 individual cohort (collected in 2016) were also measured for their cross  
134 reactivities with SARS-CoV-2 S protein. Demographical information about

135 these two cohorts was described in [Table 1](#).

136

### 137 **Detection of SARS-CoV-2 S1 and S2 specific binding antibodies**

138 In-house enzyme-linked immunosorbent assays (ELISA) were developed to  
139 measure SARS-CoV-2 S1 and S2 specific binding antibodies. High-binding  
140 96-well EIA plates (Cat# 9018, Corning, USA) were coated with purified  
141 SARS-CoV-2 S1 (Cat# 40591-V08H, Sino Biological, China) or S2 proteins  
142 (Cat# 40590-V08B, Sino Biological, China) at a final concentration of 1µg/ml in  
143 carbonate/bi-carbonate coating buffer (30mM NaHCO<sub>3</sub>, 10mM Na<sub>2</sub>CO<sub>3</sub>, pH  
144 9.6). Subsequently, the plates were blocked with 1×PBS containing 5% milk  
145 for 1 hour at 37°C. Next, 100µl of diluted human plasma or mouse serum was  
146 added to each well. After 1-hour incubation at 37°C, the plates were washed  
147 with 1×PBS containing 0.05% Tween20 for 5 times. Then, 100µl of a HRP  
148 labeled goat anti-mouse IgG antibody (Cat# ab6759, Abcam, UK) or goat  
149 anti-mouse IgG antibody (Cat# 115-035-003, Jackson Immuno Research, USA)  
150 diluted in 1×PBS containing 5% milk were added to each well and incubated  
151 for 1 hour at 37°C. After a second round of wash, 100µl of TMB substrate  
152 reagent (Cat# MG882, MESGEN, China) was added to each well. 15 minutes  
153 later, the color development was stopped by adding 100µl of 1M H<sub>2</sub>SO<sub>4</sub> to  
154 each well and the values of optical density at OD<sub>450nm</sub> and OD<sub>630nm</sub> were  
155 measured using 800 TS microplate reader (Cat# 800TS, Biotek, USA).

156

### 157 **Competitive ELISA**

158 According to the reference sequence of SARS-CoV-2 (Genebank accession  
159 number: NC\_045512), peptides (18-mer overlapping by 11 residues, purities >  
160 95%) encompass the full length of S protein were synthesized by GL Biochem  
161 (Shanghai, China). The experiment procedure was generally similar with the  
162 afore mentioned in-house ELISA assays, except that the diluted mouse serum  
163 or human plasma were incubated with synthesized peptides (5µg/ml) for 1  
164 hour at room temperature before adding into the coated EIA plates. 1×PBS  
165 containing 0.01% DMSO (the solvent used to dissolve peptides) were used as  
166 the negative control in this assay.

167

### 168 **Antibody avidity assay**

169 Avidity of Ag-specific Ab Avidity of Ag-specific Ab was determined by avidity

170 ELISA as reported (34) with minor modifications. Briefly, plates were coated as  
171 the regular ELISA assay described above. Diluted (1:200) mouse sera were  
172 added into each well. After 1-hour incubation, ELISA plates were washed with  
173 washing buffer and incubated with 1.5M NaSCN or PBS for 15 mins at room  
174 temperature and then immediately washed with washing buffer. Ab avidity  
175 index was defined as the ratio of the OD value of a sample with 1.5M NaSCN  
176 treatment versus the OD value of the same sample with PBS treatment.

177

### 178 **FACS analysis of S2 specific B cells in mice**

179 Spleen and mesenteric lymph nodes were isolated from naïve SPF mice and  
180 single-cell suspensions were freshly prepared. After counting,  $1 \times 10^6$  single  
181 cells were resuspended in 100 $\mu$ l R10 (RPMI1640 containing 10% fetal bovine  
182 serum) and incubated with biotinylated S2 protein (Cat# 40590-V08B-B, Sino  
183 Biological, China) for 30 minutes at room temperature. After incubation, the  
184 cells were washed twice with 500 $\mu$ l R10. Then, the cells were incubated with  
185 the mixture of PE-anti-mouse CD19 (Cat# 152408, Biolegend, USA, 1 $\mu$ l/test),  
186 BV510-anti-mouse CD45 (Cat# 103137, Biolegend, USA, 1.25 $\mu$ l/test) and  
187 Streptavidin-IF647 (Cat# 46006, AAT Bioquest, USA, 0.2 $\mu$ l/test) at room  
188 temperature for 30 minutes. After washing, the stained cells were resuspended  
189 in 200 $\mu$ l 1 $\times$ PBS and analyzed using a BD LSRFortessa™ Flow Cytometer.  
190 The data were analyzed using the FlowJo software (BD Biosciences, USA).

191

### 192 **Preparation of P144 specific monoclonal antibodies**

193 Monoclonal antibodies against P144 were prepared from one naïve BALB/c  
194 mouse and one naïve C57BL/6 mouse respectively using the hybridoma  
195 technique. Briefly, freshly isolated splenocytes were mixed and fused with  
196 SP2/0 cells at a ratio of 1:10. Hybridoma cell clones secreting P144 specific  
197 antibodies were screened by ELISA and monoclonal hybridoma cells were  
198 selected by multiple rounds of limited dilution. Selected clones of hybridoma  
199 cells were injected intraperitoneally into BALB/c $\times$ ICR hybrid mice. About 1-2  
200 weeks later, peritoneal fluid was collected, and monoclonal IgG was purified  
201 using Protein A resin. The purities of monoclonal antibodies were verified using  
202 SDS-PAGE and the antibody concentrations were determined using a BCA kit  
203 (Cat# P0012, Beyotime Biotechnology, China).

204



205 **Isolation of gut commensal bacteria and preparation of whole cell lysate**  
206 **(WCL)**

207 About 2g of each fecal sample was suspended with 15ml sterile 1×PBS and  
208 vortexed thoroughly to obtain uniform mixtures. After centrifugation at 200×g  
209 for 5 min, the supernatants were collected, and the sediments were discarded.  
210 This process was repeated twice. Next, all the supernatant samples were  
211 centrifuged twice at 9000×g for 5 min and the supernatants were discarded.  
212 The precipitated bacteria pellets were resuspended in 500µl of 1×PBS  
213 (containing 1mM PMSF) and disrupted with an ultrasonic cell crusher (the  
214 probe-type sonicator, Model JY92-II; Ningbo Scientz Biotechnology Co., Ltd,  
215 China). After sonication, the samples were centrifuged at 10000rpm for 30  
216 minutes to remove the cellular debris.

217

218 **Western blotting**

219 WCL containing 10µg of total protein was separated by SDS-PAGE (10%  
220 acrylamide gels) and then transferred onto a PVDF membrane (Cat#  
221 IPVH00010, Millipore, USA) or stained with Coomassie brilliant blue. After  
222 blocking with 5% skim milk for 2h, the membrane was incubated with a P144  
223 specific monoclonal antibody or a control mouse IgG at a concentration of 1  
224 µg/ml. After washing, the membrane was incubated with HRP conjugated goat  
225 anti-mouse IgG antibody (Cat # ab6759, Abcam, UK) diluted 1:5000 in TBST  
226 (Tris-buffered saline, pH 8.0, 0.05% Tween 20) containing 5% skim milk. After  
227 wash, the bands were developed with an ultra-sensitive ECL substrate (Cat#  
228 K-12045-D10, Advansta, USA). The area corresponding to the specific WB  
229 bands were excised from the gel stained with Coomassie blue and analyzed  
230 using the mass spectrometry.

231

232 **Mass spectrometry analysis**

233 The FASP digestion was adapted for the following procedures in Microcon  
234 PL-10 filters. After three-time buffer displacement with 8 M Urea and 100 mM  
235 Tris-HCl, pH 8.5, proteins were reduced by 10 mM DTT at 37 °C for 30 min and  
236 followed by alkylation with 30 mM iodoacetamide at 25°C for 45 min in dark.  
237 Digestion was carried out with trypsin (enzyme/protein as 1:50) at 37°C for 12  
238 h after a wash with 20% ACN and three-time buffer displacement with  
239 digestion buffer (30 mM Tris-HCl, pH 8.0). After digestion, the solution was

240 filtrated out and the filter was washed twice with 15% ACN, and all filtrates  
241 were pooled and vacuum-dried to reach a final concentration to 1 mg/ml.  
242 LC-MS analysis was performed using a nanoflow EASYnLC 1200 system  
243 (Thermo Fisher Scientific, Odense, Denmark) coupled to an Orbitrap Fusion  
244 Lumos mass spectrometer (Thermo Fisher Scientific, Bremen, Germany). A  
245 one-column system was adopted for all analyses. Samples were analyzed on  
246 a home-made C18 analytical column (75  $\mu\text{m}$  i.d.  $\times$  25 cm, ReproSil-Pur 120  
247 C18-AQ, 1.9  $\mu\text{m}$  (Dr. Maisch GmbH, Germany)). The mobile phases consisted  
248 of Solution A (0.1% formic acid) and Solution B (0.1% formic acid in 80% ACN).  
249 The derivatized peptides were eluted using the following gradients: 2–5% B in  
250 2 min, 5–35% B in 100 min, 35–44% B in 6 min, 44–100% B in 3 min, 100% B  
251 for 10 min, at a flow rate of 200 nl/min. Data-dependent analysis was  
252 employed in MS analysis: The time between master scan was 3s, and  
253 fragmented in HCD mode, normalized collision energy was 30.

254

### 255 **Construction and preparation of a candidate DNA vaccine encoding** 256 **SARS-CoV-2 full length S protein**

257 The full-length *s* gene sequence of the reference SARS-CoV-2 strain was  
258 optimized according to the preference of human codon usage and synthesized  
259 by GENEWIZ life science company (Suchow, China). The codon optimized  
260 spike gene was subcloned into a eukaryotic expression vector (pJW4303,  
261 kindly gifted by Dr. Shan Lu's Laboratory at the University of Massachusetts)  
262 (35). And the sequence of inserted gene was verified by Sanger sequencing  
263 (Sangon Biotech Co., Ltd., Shanghai, China). An EndoFree Plasmid  
264 Purification Kit (Cat#12391, Qiagen, Hilden, USA) was used to prepare the  
265 recombinant plasmid for mouse vaccination.

266

### 267 **Mouse vaccination**

268 Peripheral blood samples were collected from female adult mice and  
269 pre-existing S2 binding antibodies were measured using the previously  
270 described in-house ELISA method. According to their pre-existing S2 binding  
271 antibody levels (at 1:100 dilution of serum), the mice were divided into three  
272 groups: low ( $0.015 < \text{OD}_{450\text{nm}-630\text{nm}} \leq 0.130$ ,  $n=6$ ), moderate ( $0.130 <$   
273  $\text{OD}_{450\text{nm}-630\text{nm}} \leq 0.750$ ,  $n=6$ ) and high ( $\text{OD}_{450\text{nm}-630\text{nm}} > 0.750$ ,  $n=6$ ). All mice  
274 were immunized intramuscularly with the candidate S protein DNA vaccine



275 (50µg/mouse) for three times at an interval of 2 weeks. Three weeks post the  
276 third vaccination, the mice were euthanized. Peripheral blood, bronchial lavage  
277 and spleen were collected for assays of S protein specific immune responses.

278

### 279 **Metagenomic analysis of mouse gut microbiota**

280 Stool (fecal) samples were self-collected and DNA was extracted from 250 mg  
281 of each fecal sample in duplicate. The DNA samples were separated strictly  
282 according to TIANamp Stool DNA Kit (Cat# DP328, TIANGEN, China). Then, a  
283 total amount of 1µg DNA per sample was used as input material for the DNA  
284 sample preparations. Sequencing libraries were generated using NEBNext®  
285 Ultra™ DNA Library Prep Kit for Illumina (NEB, USA) following manufacturer's  
286 recommendations and index codes were added to attribute sequences to each  
287 sample. Briefly, the DNA sample was fragmented by sonication to a size of  
288 350bp, then DNA fragments were end-polished, A-tailed, and ligated with the  
289 full-length adaptor for Illumina sequencing with further PCR amplification. At  
290 last, PCR products were purified (AMPure XP system) and libraries were  
291 analyzed for size distribution by Agilent 2100 Bioanalyzer and quantified using  
292 real-time PCR. The clustering of the index-coded samples was performed on a  
293 cBot Cluster Generation System according to the manufacturer's instructions.  
294 After cluster generation, the library preparations were sequenced on an  
295 Illumina Novaseq 6000 platform and paired-end reads were generated.

296

### 297 **SARS-CoV-2 pseudo-virus neutralization assay**

298 VSV-backboned SARS-CoV-2 pseudo-viruses were prepared according to a  
299 reported method (36). The neutralization assay was conducted by following  
300 the previously described procedure (36, 37). Briefly, 100µl of serially diluted  
301 mice sera were added into 96-well cell culture plates. Then, 50µl of  
302 pseudo-viruses with a titer of 13000 TCID<sub>50</sub>/ml were added into each well and  
303 the plates were incubated at 37°C for 1 hour. Next, Vero cells were added into  
304 each well (2×10<sup>4</sup> cells/well) and the plates were incubated at 37°C in a  
305 humidified incubator with 5% CO<sub>2</sub>. 24 hours later, luminescence detection  
306 reagent (Bright-Glo™ Luciferase Assay System, Promega, USA) was added to  
307 each well following the manufacturer's instruction. The luminescence was  
308 measured using a luminescence microplate reader (GloMax®  
309 Navigator Microplate Luminometer, Promega, USA) within 5 minutes. The

310 Reed-Muench method was used to calculate the virus neutralization titer.  
311 Antibody neutralization titers were presented as 50% maximal inhibitory  
312 concentration (IC<sub>50</sub>).

313

### 314 **Detections of S protein specific cellular immune responses**

315 SARS-CoV-2 S protein specific IFN- $\gamma$  releases were measured using the  
316 method of enzyme-linked immunosorbent spot (ELISPOT) assays (Cat#  
317 551083, BD Bioscience, USA) according to a previously described  
318 procedure(38). Briefly, the 96-well ELISPOT plates were coated with purified  
319 anti-mouse IFN- $\gamma$  monoclonal antibody overnight at 4°C. Then, the plates were  
320 blocked and  $2 \times 10^5$  fresh splenocytes were added into each well and  
321 incubated with peptide pools for 20 hours at 37°C in a humidified incubator  
322 with 5% CO<sub>2</sub>. The final concentration for each peptide was 1 $\mu$ g/ml. After  
323 incubation, detecting antibody and Avidin-HRP were added sequentially.  
324 Finally, the plates were developed using the BD™ ELISPOT AEC Substrate  
325 Set (Cat#551951, BD Bioscience, USA) according to the manufacturer's  
326 manual. Spots representing IFN- $\gamma$  producing cells were enumerated using an  
327 automated ELISPOT plate reader (ChampSpot III Elispot Reader, Saizhi,  
328 Beijing, China).

329 At the same time, the supernatants in the wells of ELISPOT plates were also  
330 collected for detecting secreted cytokines using a multiplexed cytokine beads  
331 array kit (Cat# 741054, Biolegend, USA).

332

### 333 **Statistical analysis**

334 All statistical analyses were performed using GraphPad Prism 8  
335 (GraphPad Software, Inc., La Jolla, CA, USA). Comparisons between two  
336 groups were conducted by the method of *t*-test. Comparisons among three or  
337 more group were done using one-way ANOVA. *P*<0.05 was considered as  
338 statistically significant.

339

## 340 **Results**

### 341 **Pre-existing antibodies recognizing a dominant linear epitope on** 342 **SARS-CoV-2 S2 protein were detected in both human and mice**

343 Pre-existing antibodies cross-react with SARS-CoV-2 S protein have been  
344 found in uninfected individuals by multiple previous studies (22, 25, 26, 39). It

345 was postulated that the pre-existing immunities against SARS-CoV-2 might be  
346 induced by previous exposure to seasonal human coronaviruses (22, 30, 32,  
347 33, 40). However, contradictory evidence suggested that human common cold  
348 coronavirus infection did not necessarily induce antibodies cross-reactive with  
349 SARS-CoV-2 spike protein (28, 41, 42). In addition to this hypothesis, an  
350 alternative explanation suggested that the cross-reactive immunities to  
351 SARS-CoV-2 might derive from other common human pathogens and  
352 vaccines (43).

353 To track the origins of the pre-existing cross-reactive antibodies to  
354 SARS-CoV-2 spike protein, in this study, we first measured the levels of  
355 pre-existing S protein specific antibodies in healthy human individuals and  
356 SPF mice. Our data showed that the cross-reactive antibody responses  
357 against S2 were significantly stronger than those against S1 in plasma  
358 samples of healthy human collected both pre (2016 cohort) and post (2020  
359 cohort) the outbreak of COVID-19 pandemic (Fig.1A and 1B). More strikingly,  
360 our data showed that binding antibodies targeting S2 could also be detected in  
361 two strains of naïve SPF mice (Fig. 1C and 1D). And this finding was further  
362 confirmed by Western-blotting (WB) assays, which showed that mouse sera  
363 with high ELISA-detected OD values (Fig. 2A) bound specifically with purified  
364 S2 while not S1 (Fig. 2B). Quite interestingly, the WB results indicated that  
365 cross-reactive antibodies against S2 also existed in the serum of a mouse  
366 (#487) with no detectable binding signal in the S2 ELISA assay (Fig. 2A and  
367 2B). We next performed linear antibody epitope mapping using an in-house  
368 developed method of peptide competition ELISA. Our data showed that a  
369 single peptide (P144, aa1145-aa1162, 18 mer) accounted for most of the  
370 observed pre-existing antibody responses towards S2 in mice (Supplementary  
371 Figure 1). Via employing a series of truncated peptides based on P144, we  
372 determined the minimal range of this epitope  
373 (1147-SFKEELDKYFKNHT-1160), which locates on the connector domain  
374 (adjacent to the N-terminal of HR2 domain) (Fig. 2C). We also proved that  
375 antibodies recognizing this epitope widely existed in both healthy human and  
376 naïve SPF mice using the competitive ELISA assay (Fig.3).

377

378 **The P144 specific antibody responses might be engendered by**  
379 **exposures to certain commensal gut bacteria**

380 To explore the potential origins of the pre-existed P144 specific antibodies, we  
381 first performed phylogenetic analyses among SARS-CoV-2 and other human  
382 coronaviruses. The results showed that the aa sequence of P144 was highly  
383 conserved among SARS-CoV-2 variants and SARS-CoV, while the similarities  
384 between P144 and MERS-CoV or seasonal human coronaviruses were  
385 relatively low, especially within the range of predicted antibody binding epitope  
386 (boxed fragment) ([Figure 4A](#)). The possibility of coronavirus infection in our  
387 SPF-mouse colonies was excluded by serum screening tests using  
388 commercialized mouse hepatitis virus (MHV) antigen and antibody detection  
389 kits ([Data not shown](#)).

390 Subsequently, to investigate whether environmental factors contribute to the  
391 induction of these S2 cross-reactive antibodies, we compared the levels of  
392 pre-existing S2 binding antibodies between mice housed in SPF condition and  
393 mice maintained in a sterile isolation pack. Our data showed that the levels of  
394 pre-existing S2 binding antibodies were significantly higher in SPF mice  
395 ([Figure 4B](#)). Through metagenomic sequencing, we further demonstrated that  
396 the compositions of commensal gut bacteria were significantly different  
397 between mice housed in SPF condition and mice maintained in the sterile  
398 isolation pack ([Supplementary Figure 2A](#)). The abundance of bacteroidaceae,  
399 prevotellaceae and parabacteroides increased significantly in the commensal  
400 gut bacteria of SPF mice ([Figure 4C](#)). Moreover, flowcytometry assays  
401 indicated that the frequencies of S2 specific B cells (CD3<sup>-</sup>S2<sup>+</sup>CD19<sup>+</sup>) in  
402 mesenteric lymph nodes were significantly higher than those in spleen  
403 ([Supplementary Figure 2B](#)). These results collectively implied that the S2  
404 cross-reactive antibodies might be induced by exposures to certain microbial  
405 antigens.

406

407 **P144 specific monoclonal antibodies reacted with commensal gut**  
408 **bacteria from both human and mouse and showed limited neutralizing**  
409 **activities**

410 To probe the potential antigens that might induce the P144 binding antibodies,  
411 we isolated 6 mAbs from two naïve SPF mice (one C57BL/6J mouse and one  
412 BALB/c mouse) with high levels of pre-existing S2 specific antibody responses.  
413 Five of these mAbs recognized P144 solely, while one mAb (clone M3) bound  
414 with P144 and P103 simultaneously ([Supplementary Figure 3](#)). Results of

415 competitive ELISA showed that the minimal epitopes varied slightly among the  
416 five P144 specific mAbs, especially at the C-terminal of P144 ([Supplementary](#)  
417 [Figure 3A](#)). The neutralizing potentials of these isolated monoclonal antibodies  
418 were evaluated using a pseudo virus-based neutralization assay. Our results  
419 showed that these monoclonal antibodies exhibited limited neutralizing activity  
420 against 5 major SARS-CoV-2 variants ([Supplementary Figure 4](#)). Of note, G18  
421 neutralized the Indian strain (B.1.617) by 31%; F5 neutralized the UK strain  
422 (B.1.1.7) and the South African strain (B.1.351) by around 20%; G13  
423 neutralized the South African strain (B.1.351) by nearly 20% ([Supplementary](#)  
424 [Figure 4](#)).

425 To prove the cross-reactivities between S2 and commensal gut microbial  
426 antigens, whole cell lysates (WCL) of mouse and human commensal gut  
427 bacteria were prepared and used as antigens for Western blotting assays,  
428 respectively. As shown in [Figure 5A](#), specific bindings with the WCL of mixed  
429 fecal bacteria prepared from mice either with low levels of pre-existing  
430 antibodies (L) or with high levels of pre-existing antibodies (H) could be clearly  
431 visualized for each isolated mAbs. It was noteworthy that all mAbs except E10  
432 strongly recognized a band around 180KD in the sample from mice with high  
433 pre-existing antibody responses. E10 predominantly recognized a band  
434 around 55KD in both samples, while stronger binding with the sample from  
435 mice with high pre-existing antibody responses could be visually observed  
436 ([Figure 5A](#)). Among the six mAbs, F5 showed the most diverse binding  
437 compacity. In addition to the band around 180KD, F5 bound with a band  
438 around 55KD (similar with E10) and a band between 40KD-55KD ([Figure 5A](#)).  
439 In comparison with the WB results of mouse samples, the recognized bands  
440 were less consistent across different human fecal bacteria samples ([Figure](#)  
441 [5B](#)), presumably due to the individual to individual variation of gut microbiota  
442 composition. We found that a band around 70KD was recognized by most  
443 mAbs in 4 (lanes 1, 5, 6, 7) out of 7 samples and a band between 50KD-70KD  
444 was recognized by all mAbs in 3 (Lanes 2, 3, 7) out 7 samples. Besides, our  
445 data showed that the recognition pattern of each sample was largely  
446 consistent across different mAbs ([Figure 5B](#)).

447 Proteins corresponding to specifically recognized bands were excised from  
448 Coomassie blue stained gels and analyzed by the mass spectrometry. For the  
449 mouse fecal bacteria samples, protein bands with molecular weights around

450 180KD, 100KD, 55KD-70KD and 40KD-55KD (indicated by arrows in Figure  
451 5A, panel F5) were selected. For human fecal bacteria samples, protein bands  
452 with molecular weights around 50KD-70KD, 70KD and 70KD-100KD  
453 (indicated by arrows in Figure 5B, panel F5) were selected. The lists of  
454 proteins identified in mouse and human samples were shown in [Table 2](#) and  
455 [Table 3](#), respectively. Proteins with molecular weights corresponding  
456 approximately to the excised protein bands were identified for both human and  
457 mouse fecal bacteria samples. Of note, multiple proteins within the theoretical  
458 MW range of 58KD to 60KD were found to be identical between mouse and  
459 human samples, which included Fumarate hydratase class I (Accession#  
460 P14407), Formate-tetrahydrofolate ligase OS (Accession# Q189R2),  
461 Phosphoenolpyruvate carboxykinase (ATP) OS (Accession# C4ZBL1 and  
462 A6LFQ4) and 60 kDa chaperonin OS (Accession# A0Q2T1).

463

#### 464 **Pre-existing cross-reactive antibodies impacted specific immunities** 465 **induced by a candidate DNA vaccine encoding SARS-CoV-2 S protein**

466 Pre-existing antibodies has been shown to be able to shape the recall immune  
467 responses upon influenza infection and vaccination (6). And the concern about  
468 how the pre-existing immunities may influence the effect of a SARS-CoV-2  
469 vaccine has also attracted lots of attention (33). To investigate the impact of  
470 the pre-existing P144 antibodies on the immunogenicity of a candidate DNA  
471 vaccine, 18 BALB/c mice were divided into 3 groups according to their levels of  
472 pre-existing S2 binding antibodies and immunized with a DNA vaccine  
473 encoding the full length of SARS-CoV-2 S protein ([Figure 6A and 6B](#)). Our data  
474 showed that mice with high levels of pre-existing S2 binding antibodies  
475 mounted significantly higher S2 binding antibody responses after vaccination  
476 compared to mice with low or moderate levels of pre-existing S2 binding  
477 antibodies ([Figure 6C](#)). More specifically, the average level of P144 specific  
478 antibody responses was also stronger in mice with high levels of pre-existing  
479 S2 binding antibodies than mice with low levels of pre-existing S2 binding  
480 antibodies ([Figure 6D and 6E](#)). By comparison, both the S1 binding antibody  
481 and the neutralizing antibody titers did not significantly differ among all groups,  
482 despite that mice with moderate or high levels of pre-existing antibodies  
483 tended to mount higher average titer of S1 binding antibodies ([Figure 6F and](#)  
484 [6G](#)). Mice without vaccination showed neither obvious S1 binding antibody



485 response nor neutralizing activity ([Data not shown](#)). We further investigated  
486 the influence of pre-existing antibodies on humoral immune responses in  
487 mouse respiratory tract after vaccination. And our data showed that the levels  
488 of S1 specific IgG in BALF were similar among the three groups after DNA  
489 vaccination ([Figure 7A](#)), while the average level of S2 specific IgG in BALF  
490 from mice with high pre-existing S2 binding antibodies was significantly higher  
491 than those from mice with low pre-existing antibodies ([Figure 7B](#)). S protein  
492 specific IgA response did not increase significantly after vaccination as  
493 compared with unvaccinated group ([Figure 7C and 7D](#)).

494 As most pre-existing antibodies in naïve SPF mice recognized P144 ([Figure](#)  
495 [2C and Supplementary Figure 1](#)), we delineated the impact of pre-existing  
496 antibody on the epitope recognition after vaccination. Our results showed that  
497 the minimum epitope recognition pattern by the sera of mice with high levels of  
498 pre-existing antibodies remained unchanged after vaccination ([Figure 8](#)).  
499 Whereas the minimum epitope recognized by the sera of mice with moderate  
500 and low levels of pre-existing antibody responses altered at either the  
501 N-terminal or both terminals of P144 ([Figure 8](#)).

502 In addition to antibody measurement, we compared S protein specific T cell  
503 responses among the three groups as well ([Figure 9A](#)). The results showed  
504 that the candidate DNA vaccine elicited robust S protein specific T cell  
505 responses in all groups ([Figure 9](#)). Although no statistical significance was  
506 reached, interesting trends were observed: First, mice with high levels of  
507 pre-existing S2 binding antibodies tended to mount relatively higher S1  
508 specific cellular immune responses ([Figure 9B, 9C and 9D](#)); second, as  
509 measured by the total responses of IL-6, IL-2 and TNF- $\alpha$ , mice with high levels  
510 of pre-existing antibodies tended to mount stronger T cell responses against  
511 S1 while lower responses against S2 ([Figure 9C and 9D](#)). Mice without  
512 vaccination showed no S protein specific T cells responses ([Data not shown](#)).

513

## 514 **Discussion**

515 The origins of pre-existing cross-reactive immunities against SARS-CoV-2  
516 have been investigated vigorously since the outbreak of the pandemic ([44](#)).  
517 Accumulating data suggest that cross-reactive T cells ([33, 45-48](#)) in  
518 SARS-CoV-2 unexposed human might be induced by previous infections of  
519 other hCoVs. While the origins of pre-existing cross-reactive antibodies could

520 not be completely explained by previous infections of other coronaviruses, as  
521 recent studies revealed that the magnitude of antibody responses to  
522 SARS-CoV-2 S protein in the sera of patients with COVID-19 was not related  
523 to HCoVs' S titers (49) and immunization with coronaviruses OC43 did not  
524 induce significant SARS-CoV-2 S protein cross-reactive antibodies in mice.  
525 Moreover, it has also been observed that SARS-CoV-2 S protein specific  
526 binding antibody responses were weak in SARS-CoV-2 unexposed individuals  
527 with obvious binding antibody responses against S proteins of common cold  
528 hCoVs (50, 51).

529 To track the potential origins of the pre-existed cross-reactive antibodies  
530 targeting SARS-CoV-2 spike protein, in this study, we first screened the  
531 cross-reactive antibody responses in SARS-CoV-2 unexposed human plasma  
532 collected in 2020 and 2016, respectively. In both cohorts, we found that the  
533 magnitudes of S2 binding antibodies were significantly higher than those of S1  
534 binding antibodies. This finding is consistent with previous studies showing  
535 that pre-existing S2 cross-reactive antibody responses are stronger than S1  
536 cross-reactive antibody responses in SARS-CoV-2 unexposed individuals (49,  
537 52, 53). Since S2 cross-reactive antibody responses have also been observed  
538 in unexposed animals (49), we continued to screen the cross-reactive antibody  
539 responses in two strains of naïve SPF mice. Our data showed that the OD  
540 values of S2 cross-reactive antibodies were significantly higher than those of  
541 S1 cross-reactive antibodies in naïve BALB/c and C57BL/6 mice. Detections of  
542 mouse sera collected from another two independent SPF animal facilities  
543 confirmed this finding (Data not shown). We also tried to detect the  
544 SARS-CoV-2 S protein specific T cells responses in mice with high  
545 pre-existing S2 cross-reactive antibodies using the IFN- $\gamma$  ELISPOT assay,  
546 which showed that there was no pre-existing cross-reactive T cell response.

547 To facilitate the search of potential antigens that induced the cross-reactive  
548 antibodies, we identified a dominant antibody epitope (P144) through a  
549 method of competitive ELISA based linear antibody epitope mapping. P144 is  
550 located within the connector domain of S2 (aa1147-aa1160, directly N-terminal  
551 of the HR2 region). The same epitope has been predicted (43) and detected in  
552 both SARS-CoV-2 unexposed and infected individuals by multiple previous  
553 studies (22, 23, 25, 26, 32). In this study, we also detected P144 specific  
554 antibody responses in plasma of healthy individuals collected in both 2020 and

555 2016. More interestingly, we found that the pre-existing S2 cross-reactive  
556 antibodies in mice were predominantly against the single epitope. Of note,  
557 although the aa sequence of P144 is highly conserved between SARS-CoV-2  
558 and SARS-CoV, its similarity with four seasonal hCoVs is relatively low. A  
559 recent study showed that this epitope was more frequently recognized than its  
560 homologous peptides from common cold hCoVs by antibodies in plasma of  
561 COVID-19 negative individuals (23). The above evidence implied again that  
562 the pre-existing S2 specific antibodies might not be necessarily elicited by  
563 previous common cold coronavirus infections.

564 As the pre-existing S2 binding antibodies in mice were predominantly against  
565 P144, it provided us a good chance to unveil their origins. To do so, we first  
566 labeled mouse B cells with purified S2 protein and found that the frequency of  
567 S2 specific B cells was significantly higher in mesenteric LN than in spleen,  
568 suggesting that the gastrointestinal tract might be the primary site where the  
569 cross-reactive B cells were activated. Exposure to a certain gut microbial  
570 antigen, which can promote B cell diversification and stimulate antibody  
571 production in both T-dependent and -independent ways (54), might account for  
572 the presence of the cross-reactive antibodies. To prove this hypothesis, we  
573 next compared the levels of pre-existing S2 cross-reactive antibodies between  
574 mice housed in a sterile isolation pack and mice maintained in SPF condition.  
575 Our results showed that the levels of pre-existing S2 cross-reactive antibodies  
576 were significantly higher in SPF mice. Through metagenomic sequencing, we  
577 further demonstrated that the abundance of bacteroidaceae, prevotellaceae  
578 and parabacteroides were also significantly higher in the commensal gut  
579 bacteria of SPF mice. Therefore, we speculated that the S2 cross-reactive  
580 antibodies might be induced by commensal gut bacteria.

581 To prove the above speculation directly, we isolated six P144 specific  
582 monoclonal antibodies from a naïve BALB/c mouse and a naïve C57BL/6  
583 mouse, respectively. All the six mAbs were confirmed to be able to bind with  
584 P144 and showed weak neutralizing capacities against five SARS-CoV-2  
585 variants. By leveraging these mAbs, we detected the potential cross-reactive  
586 antigens in mouse and human fecal microbiota through WB assays. Compared  
587 with a control mouse IgG, specific bands were observed for each mAb, which  
588 proved antibody cross-reactivities between SARS-CoV-2 and commensal gut  
589 bacteria. The strongly recognized protein bands were further analyzed by

590 LC-MS. Our data showed that antigens derived from bacteroides and  
591 parabacteroides were frequently identified in fecal bacteria samples of both  
592 human and mouse, which was in consistence with our metagenomic  
593 sequencing data showing that the abundance of bacteroides and  
594 parabacteroides was significantly higher in the commensal gut bacteria of mice  
595 with high pre-existing S2 binding antibody levels. More intriguingly, five  
596 potential cross-reactive microbial antigens were identified in mouse and  
597 human samples simultaneously, which implied that the S2 cross-reactive  
598 antibodies might naturally occur in different species of mammals. We analyzed  
599 the sequence similarities between P144 and the proteins identified by LC-MS.  
600 Our results showed that most identified proteins shared 40%-70% identities for  
601 more than 8 residues with P144 ([Data not shown](#)). The cross-reactive epitopes  
602 on the identified proteins could not specified based on current data. Besides,  
603 the neutralizing mechanism(s) of P144 specific antibodies and their potential  
604 influences on gut microbiota were not clarified in this study. We plan to look  
605 into these issues in future.

606 In parallel with tracking the initial antigens that induced the S2 cross-reactive  
607 antibodies, we investigated the impact of pre-existing antibodies on the  
608 immunogenicity of a candidate DNA vaccine as well. According to previous  
609 reports, pre-existing cross-reactive antibodies may influence the effects of  
610 different vaccines differentially ([6](#), [55](#)). In this study, our data showed that the  
611 pre-existing cross-reactive antibodies shaped the vaccine-induced immune  
612 responses by promoting S2 binding antibodies in both peripheral blood and  
613 bronchial lavage. Meanwhile, the production of SARS-CoV-2 neutralizing  
614 antibodies was not impaired. Through epitope mapping, we further showed  
615 that the pre-existing antibodies strongly imprinted the minimal epitope  
616 recognition in mice with high levels of pre-existing antibodies, which suggested  
617 that the influence of pre-existing cross-reactive antibodies on vaccine induced  
618 antibody responses was primarily epitope specific. In addition to antibody  
619 response, we also found that the high levels of pre-existed S2 binding  
620 antibodies tended to induce higher S1 specific T cell responses while lower S2  
621 specific T cell responses, which indicated that the pre-existing cross-reactive  
622 antibodies might change the balance between humoral versus cellular immune  
623 responses. Collectively, the above results manifested that the pre-existing  
624 cross-reactive antibodies against SARS-CoV-2 S2 did not impair the

625 immunogenicity of the candidate DNA vaccine. Further experiments of live  
626 virus challenge will help to clarify whether the increased T cell and S2 binding  
627 antibody responses may mitigate the severity of disease caused by  
628 SARS-CoV-2.

629 A deep understanding of pre-existing cross-reactive antibodies against  
630 SARS-CoV-2 will enable better therapeutic, diagnostic and vaccine strategies.  
631 In this study, we provided evidence showing that antibodies targeting a  
632 conserved linear epitope on S2 cross-reacted with gut microbial antigens from  
633 both human and mouse, manifesting that some of the pre-existing  
634 cross-reactive antibodies might be induced by exposure to certain commensal  
635 gut bacteria. We proved that the pre-existing S2 cross-reactive antibodies did  
636 not impair the immunogenicity of a candidate DNA vaccine in a mouse model.  
637 Further investigations into the role of P144 specific antibody after  
638 SARS-CoV-2 infection and its impact on gut microbiota might provide clues to  
639 elucidate the mechanisms underlying the gastrointestinal symptom of  
640 COVID-19 (56-58).

641

#### 642 **Acknowledgements**

643 We thank Miss Zhangyufan He from Huashan Hospital, Fudan University, for  
644 her kind help with the language polishing. This work was funded by the  
645 National Natural Science Foundation of China (Grant No. 81971559,  
646 82041010, 81971900, 31872744), National Science and Technology Major  
647 Project (Grant No. 2018ZX10731301-004, 2018ZX10302302-002 and  
648 2018ZX10301-404-002-003) and the Science and Technology Commission of  
649 Shanghai Municipality (Grant No. 20411950400).

650

#### 651 **Author contributions**

652 Y.M.W., Y.X., C.Q., Z.Q.Z. and W.H.Z. designed the study. L.Q.J., S.F.W.,  
653 Y.M.W., X.X.T., Y.F.Z., J.W., X.Y.W., and J.W. conducted the experiments.  
654 Y.M.W., L.Q.J. and S.F.W. analyzed the data and drafted the manuscript.  
655 Y.M.W., Y.X., C.Q., Z.Q.Z. and W.H.Z. revised the manuscript. D.M.Y. and  
656 W.H.W. provided intellectual inputs in tackling technical challenges in tracking  
657 the potential cross-reacting antigens.

658

## 659 **Conflict of Interest**

660 The authors declare that they have no relevant conflicts of interest.

661

## 662 **References**

- 663 1. Lu LL, Suscovich TJ, Fortune SM, Alter G. Beyond binding: antibody effector functions in  
664 infectious diseases. *Nature reviews Immunology*. 2018;18(1):46-61.
- 665 2. Warter L, Appanna R, Fink K. Human poly- and cross-reactive anti-viral antibodies and their  
666 impact on protection and pathology. *Immunologic research*. 2012;53(1-3):148-61.
- 667 3. Cobey S, Hensley SE. Immune history and influenza virus susceptibility. *Current opinion in*  
668 *virology*. 2017;22:105-11.
- 669 4. Mok DZL, Chan KR. The Effects of Pre-Existing Antibodies on Live-Attenuated Viral Vaccines.  
670 *Viruses*. 2020;12(5).
- 671 5. Zimmermann P, Curtis N. Factors That Influence the Immune Response to Vaccination. *Clinical*  
672 *microbiology reviews*. 2019;32(2).
- 673 6. Dugan HL, Guthmiller JJ, Arevalo P, Huang M, Chen YQ, Neu KE, et al. Preexisting immunity  
674 shapes distinct antibody landscapes after influenza virus infection and vaccination in humans. *Science*  
675 *translational medicine*. 2020;12(573).
- 676 7. Zhang A, Stacey HD, Mullarkey CE, Miller MS. Original Antigenic Sin: How First Exposure  
677 Shapes Lifelong Anti-Influenza Virus Immune Responses. *Journal of immunology (Baltimore, Md :*  
678 *1950)*. 2019;202(2):335-40.
- 679 8. Boes M. Role of natural and immune IgM antibodies in immune responses. *Molecular*  
680 *immunology*. 2000;37(18):1141-9.
- 681 9. Auladell M, Jia X, Hensen L, Chua B, Fox A, Nguyen THO, et al. Recalling the Future:  
682 Immunological Memory Toward Unpredictable Influenza Viruses. *Frontiers in immunology*.  
683 2019;10:1400.
- 684 10. St. John AL, Rathore APS. Adaptive immune responses to primary and secondary dengue virus  
685 infections. *Nature Reviews Immunology*. 2019;19(4):218-30.
- 686 11. Izmirlly AM, Alturki SO, Alturki SO, Connors J, Haddad EK. Challenges in Dengue Vaccines  
687 Development: Pre-existing Infections and Cross-Reactivity. 2020;11(1055).
- 688 12. Andrade P, Gimblet-Ochieng C, Modirian F, Collins M, Cárdenas M, Katzelnick LC, et al. Impact  
689 of pre-existing dengue immunity on human antibody and memory B cell responses to Zika. *Nature*  
690 *Communications*. 2019;10(1):938.
- 691 13. Liao HX, Chen X, Munshaw S, Zhang R, Marshall DJ, Vandergrift N, et al. Initial antibodies  
692 binding to HIV-1 gp41 in acutely infected subjects are polyreactive and highly mutated. *The Journal of*  
693 *experimental medicine*. 2011;208(11):2237-49.
- 694 14. Bonsignori M, Liao HX, Gao F, Williams WB, Alam SM, Montefiori DC, et al. Antibody-virus  
695 co-evolution in HIV infection: paths for HIV vaccine development. *Immunological reviews*.  
696 2017;275(1):145-60.
- 697 15. Williams WB, Liao HX, Moody MA, Kepler TB, Alam SM, Gao F, et al. HIV-1 VACCINES.  
698 Diversion of HIV-1 vaccine-induced immunity by gp41-microbiota cross-reactive antibodies. *Science*  
699 (New York, NY). 2015;349(6249):aab1253.
- 700 16. Zitvogel L, Ayyoub M, Routy B, Kroemer G. Microbiome and Anticancer Immunosurveillance.



- 701 Cell. 2016;165(2):276-87.
- 702 17. Leng Q, Tarbe M, Long Q, Wang F. Pre-existing heterologous T-cell immunity and neoantigen  
703 immunogenicity. *Clinical & translational immunology*. 2020;9(3):e01111.
- 704 18. Sioud M. T-cell cross-reactivity may explain the large variation in how cancer patients respond to  
705 checkpoint inhibitors. *Scandinavian journal of immunology*. 2018;87(3).
- 706 19. Rose NR. Negative selection, epitope mimicry and autoimmunity. *Current opinion in immunology*.  
707 2017;49:51-5.
- 708 20. Anderson EM, Goodwin EC, Verma A, Arevalo CP, Bolton MJ, Weirick ME, et al. Seasonal  
709 human coronavirus antibodies are boosted upon SARS-CoV-2 infection but not associated with  
710 protection. *Cell*. 2021.
- 711 21. Galipeau Y, Greig M, Liu G, Driedger M, Langlois MA. Humoral Responses and Serological  
712 Assays in SARS-CoV-2 Infections. *Frontiers in immunology*. 2020;11:610688.
- 713 22. Klompus S, Leviatan S, Vogl T, Kalka IN, Godneva A, Shinar E, et al. Cross-reactive antibody  
714 responses against SARS-CoV-2 and seasonal common cold coronaviruses. 2020:2020.09.01.20182220.
- 715 23. Shrock E, Fujimura E, Kula T, Timms RT, Lee IH, Leng Y, et al. Viral epitope profiling of  
716 COVID-19 patients reveals cross-reactivity and correlates of severity. *Science (New York, NY)*.  
717 2020;370(6520).
- 718 24. Ortega N, Ribes M, Vidal M, Rubio R, Aguilar R, Williams S, et al. Seven-month kinetics of  
719 SARS-CoV-2 antibodies and protective role of pre-existing antibodies to seasonal human  
720 coronaviruses on COVID-19. 2021:2021.02.22.21252150.
- 721 25. Ladner JT, Henson SN, Boyle AS, Engelbrekton AL, Fink ZW, Rahee F, et al. Epitope-resolved  
722 profiling of the SARS-CoV-2 antibody response identifies cross-reactivity with endemic human  
723 coronaviruses. *Cell reports Medicine*. 2021;2(1):100189.
- 724 26. Ng KW, Faulkner N, Cornish GH, Rosa A, Harvey R, Hussain S, et al. Preexisting and de novo  
725 humoral immunity to SARS-CoV-2 in humans. *Science (New York, NY)*. 2020;370(6522):1339-43.
- 726 27. Yang R, Lan J, Huang B, A R, Lu M, Wang W, et al. Lack of antibody-mediated cross-protection  
727 between SARS-CoV-2 and SARS-CoV infections. *EBioMedicine*. 2020;58:102890.
- 728 28. Lv H, Wu NC, Tsang OT, Yuan M, Perera R, Leung WS, et al. Cross-reactive Antibody Response  
729 between SARS-CoV-2 and SARS-CoV Infections. *Cell reports*. 2020;31(9):107725.
- 730 29. Zhu Y, Yu D, Han Y, Yan H, Chong H, Ren L, et al. Cross-reactive neutralization of SARS-CoV-2  
731 by serum antibodies from recovered SARS patients and immunized animals. *Science advances*.  
732 2020;6(45).
- 733 30. Lipsitch M, Grad YH, Sette A, Crotty S. Cross-reactive memory T cells and herd immunity to  
734 SARS-CoV-2. *Nature reviews Immunology*. 2020;20(11):709-13.
- 735 31. Sumbul B, Sumbul HE, Okyay RA, Gülümsek E, Şahin AR, Boral B, et al. Is there a link between  
736 pre-existing antibodies acquired due to childhood vaccinations or past infections and COVID-19? A  
737 case control study. *PeerJ*. 2021;9:e10910.
- 738 32. Majdoubi A, Michalski C, O'Connell SE, Dada S, Narpala SR, Gelinat JP, et al. A majority of  
739 uninfected adults show pre-existing antibody reactivity against SARS-CoV-2. *JCI insight*. 2021.
- 740 33. Sette A, Crotty S. Pre-existing immunity to SARS-CoV-2: the knowns and unknowns. *Nature*  
741 *reviews Immunology*. 2020;20(8):457-8.
- 742 34. Fan W, Wan Y, Li Q. Interleukin-21 enhances the antibody avidity elicited by DNA prime and  
743 MVA boost vaccine. *Cytokine*. 2020;125:154814.
- 744 35. Lu S, Manning S, Arthos J. Antigen engineering in DNA immunization. *Methods in molecular*

- 745 medicine. 2000;29:355-74.
- 746 36. Nie J, Li Q, Wu J, Zhao C, Hao H, Liu H, et al. Establishment and validation of a pseudovirus  
747 neutralization assay for SARS-CoV-2. *Emerging microbes & infections*. 2020;9(1):680-6.
- 748 37. Li Q, Wu J, Nie J, Zhang L, Hao H, Liu S, et al. The Impact of Mutations in SARS-CoV-2 Spike  
749 on Viral Infectivity and Antigenicity. *Cell*. 2020;182(5):1284-94.e9.
- 750 38. Ren Y, Wang N, Hu W, Zhang X, Xu J, Wan Y. Successive site translocating inoculation  
751 potentiates DNA/recombinant vaccinia vaccination. *Scientific reports*. 2015;5:18099.
- 752 39. Tso FY, Lidenge SJ, Peña PB, Clegg AA, Ngowi JR, Mwaiselage J, et al. High prevalence of  
753 pre-existing serological cross-reactivity against severe acute respiratory syndrome coronavirus-2  
754 (SARS-CoV-2) in sub-Saharan Africa. *International journal of infectious diseases : IJID : official  
755 publication of the International Society for Infectious Diseases*. 2021;102:577-83.
- 756 40. Lee CH, Pinho MP, Buckley PR, Woodhouse IB, Ogg G, Simmons A, et al. Potential CD8+ T Cell  
757 Cross-Reactivity Against SARS-CoV-2 Conferred by Other Coronavirus Strains. *Frontiers in  
758 immunology*. 2020;11:579480.
- 759 41. Freeman B, Lester S, Mills L, Rasheed MAU, Moye S, Abiona O, et al. Validation of a  
760 SARS-CoV-2 spike protein ELISA for use in contact investigations and sero-surveillance.  
761 2020:2020.04.24.057323.
- 762 42. Post N, Eddy D, Huntley C, van Schalkwyk MCI, Shrotri M, Leeman D, et al. Antibody response  
763 to SARS-CoV-2 infection in humans: A systematic review. *PloS one*. 2020;15(12):e0244126.
- 764 43. Reche PA. Potential Cross-Reactive Immunity to SARS-CoV-2 From Common Human Pathogens  
765 and Vaccines. *Frontiers in immunology*. 2020;11:586984.
- 766 44. Doshi P. Covid-19: Do many people have pre-existing immunity? 2020;370:m3563.
- 767 45. Steiner S, Sotzny F, Bauer S, Na I-K, Schmueck-Henneresse M, Corman VM, et al. HCoV- and  
768 SARS-CoV-2 Cross-Reactive T Cells in COVID Patients. 2020;11(3347).
- 769 46. Mateus J, Grifoni A, Tarke A, Sidney J, Ramirez SI, Dan JM, et al. Selective and cross-reactive  
770 SARS-CoV-2 T cell epitopes in unexposed humans. 2020;370(6512):89-94.
- 771 47. Grifoni A, Weiskopf D, Ramirez SI, Mateus J, Dan JM, Moderbacher CR, et al. Targets of T Cell  
772 Responses to SARS-CoV-2 Coronavirus in Humans with COVID-19 Disease and Unexposed  
773 Individuals. *Cell*. 2020;181(7):1489-501.e15.
- 774 48. Braun J, Loyal L, Frentsch M, Wendisch D, Georg P, Kurth F, et al. SARS-CoV-2-reactive T cells  
775 in healthy donors and patients with COVID-19. *Nature*. 2020;587(7833):270-4.
- 776 49. Kim H, Seiler P, Jones JC, Ridout G, Camp KP, Fabrizio TP, et al. Antibody Responses to  
777 SARS-CoV-2 Antigens in Humans and Animals. *Vaccines*. 2020;8(4).
- 778 50. Anderson EM, Goodwin EC, Verma A, Arevalo CP, Bolton MJ, Weirick ME, et al. Seasonal  
779 human coronavirus antibodies are boosted upon SARS-CoV-2 infection but not associated with  
780 protection. *Cell*. 2021;184(7):1858-64.e10.
- 781 51. Song G, He W-t, Callaghan S, Anzanello F, Huang D, Ricketts J, et al. Cross-reactive serum and  
782 memory B-cell responses to spike protein in SARS-CoV-2 and endemic coronavirus infection. *Nature  
783 Communications*. 2021;12(1):2938.
- 784 52. Fraley E, LeMaster C, Banerjee D, Khanal S, Selvarangan R, Bradley T. Cross-reactive antibody  
785 immunity against SARS-CoV-2 in children and adults. *Cellular & molecular immunology*. 2021:1-3.
- 786 53. Nguyen-Contant P, Embong AK, Kanagaiah P, Chaves FA, Yang H, Branche AR, et al. S  
787 Protein-Reactive IgG and Memory B Cell Production after Human SARS-CoV-2 Infection Includes  
788 Broad Reactivity to the S2 Subunit. *mBio*. 2020;11(5).

789 54. Zhao Q, Elson CO. Adaptive immune education by gut microbiota antigens. *Immunology*.  
790 2018;154(1):28-37.

791 55. Bradt V, Malafa S, von Braun A, Jarmer J, Tsouchnikas G, Medits I, et al. Pre-existing yellow  
792 fever immunity impairs and modulates the antibody response to tick-borne encephalitis vaccination.  
793 *NPJ vaccines*. 2019;4:38.

794 56. Lee IC, Huo TI, Huang YH. Gastrointestinal and liver manifestations in patients with COVID-19.  
795 *Journal of the Chinese Medical Association : JCMA*. 2020;83(6):521-3.

796 57. Jin X, Lian JS, Hu JH, Gao J, Zheng L, Zhang YM, et al. Epidemiological, clinical and virological  
797 characteristics of 74 cases of coronavirus-infected disease 2019 (COVID-19) with gastrointestinal  
798 symptoms. *Gut*. 2020;69(6):1002-9.

799 58. Mao R, Qiu Y, He JS, Tan JY, Li XH, Liang J, et al. Manifestations and prognosis of  
800 gastrointestinal and liver involvement in patients with COVID-19: a systematic review and  
801 meta-analysis. *The lancet Gastroenterology & hepatology*. 2020;5(7):667-78.

802

803

804

805

806

807

808

809

810

811

812

813

814

815

816

817

818

819

820

821

822

823

824

825

826

827

828

829

830

831

832

833 **Figure legends**

834

835 **Figure 1. Pre-existing cross-reactive antibodies against SARS-CoV-2 S**  
836 **protein observed in both healthy human and naïve SPF mice**  
837 **predominantly targeted S2**

838 The pre-existing cross-reactive antibodies against S1 and S2 were measured  
839 using an in-house ELISA (Sample dilution factor: 100). **(A)** Plasma samples of  
840 healthy individuals collected in 2020 (n=95). **(B)** Plasma samples of healthy  
841 individuals collected in 2016 (n=78). **(C)** Sera of naïve C56BL/6J mice (n=12).  
842 **(D)** Sera of naïve BALB/c mice (n=101). The dot lines showed the threshold of  
843 background (3 folds of the background OD). Statistical analyses were  
844 performed using the method of paired t-test.

845

846 **Figure 2 The pre-existing S protein binding antibodies in naïve SPF mice**  
847 **recognized S2 exclusively and a dominant linear antibody epitope was**  
848 **identified on the connector domain**

849 The pre-existing S1 and S2 cross-reactive antibody levels of 6 mice selected  
850 for WB assays were shown in **(A)**. **(B)** Western-blotting assays of pre-existing  
851 cross-reactive antibodies for 6 selected mouse serum samples. The purities of  
852 S1 and S2 proteins were shown by coomassie blue staining. **(C)** The minimal  
853 epitope of P144 was defined using a method of competitive ELISA (Data  
854 shown as mean±SD, n=5). Purified S2 protein was used as the coating antigen  
855 and truncated peptides derived from P144 were used as competitors. The  
856 decreases of competitive inhibition reflected the necessity of each amino acid  
857 for the epitope recognition. Statistical differences among groups was analyzed  
858 using One-way ANOVA. \*\*\*\*, P<0.0001. M: molecular weight markers; SP,  
859 signal peptide; RBD, receptor-binding domain; FP, fusion peptide; HR, heptad  
860 repeat; CH, central helix; CD, connector domain; TM, transmembrane domain;  
861 CT, cytoplasmic tail.

862

863 **Figure 3 Cross-reactive antibodies recognizing epitope P144 widely**  
864 **existed in both healthy human and naïve SPF mice**

865 P144 specific binding antibodies were detected using a method of competitive  
866 ELISA. **(A)** For the detections of P144 specific binding antibodies in naïve SPF  
867 mice, purified S2 protein was used as the coating antigen and P144 peptide

868 was used as the competitor. **(B)** For the detections of P144 specific binding  
869 antibodies in healthy individuals, purified BSA-P144 conjugate was used as  
870 the coating antigen and P144 peptide was used as the competitor. In both  
871 experiments, the reduction of OD value reflected the presence of P144 binding  
872 antibodies.

873

874 **Figure 4 The generation of the pre-existing S2 cross-reactive antibodies**  
875 **might be associated with commensal gut microbiota**

876 **(A)** Phylogenetic analyses of the spike protein sequences of SARS-CoV-2  
877 variants, SARS-CoV, MERS-CoV and seasonal human coronaviruses. The  
878 sequence accession numbers are as follows, SARS-CoV-2 Wuhan,  
879 YP\_009724390; sequences of B.1.1.7, D614G, B.1.351, B.1.525, B.1.617 and  
880 P.1(B.1.1.281) were obtained from Global Initiative on Sharing Avian Influenza  
881 Data (GISAID); SARS-CoV, NP\_828851.1; MERS-CoV, QFQ59587.1;  
882 HCoV-OC43, QDH43719.1; HCoV-NL63, AKT07952.1; HCoV-229E,  
883 AOG74783.1; HCoV-HKU1, YP\_173238.1. Boxed fragments represent IEDB  
884 predicted linear antibody epitope (<http://tools.iedb.org/bcell/>). **(B)** Comparison  
885 of the levels of S2 specific pre-existing antibodies between naïve mice  
886 maintained under SPF condition and mice in a sterile isolation pack. **(C)**  
887 Comparison of commensal gut bacteria compositions between mice housed in  
888 a SPF facility and mice in a sterile isolation pack by metagenomic sequencing.  
889 Differences of bacterial abundance was analyzed by linear discriminant  
890 analysis (LDA) analysis and shown as the histogram of LDA scores. It was  
891 considered a significant effect size with LDA score > 4.0. (p), Phylum. (c),  
892 Class. (o), Order. (f), Family. (g), Genus. (s), Species.

893

894 **Figure 5 P144 specific monoclonal antibodies isolated from naïve SPF**  
895 **mice cross-reacted with commensal gut bacteria from both human and**  
896 **mouse**

897 Cross-reactivities between P144 specific mAbs and gut microbial antigens  
898 were detected using WB assays. A purified mouse IgG was used as the control.  
899 **(A)** WB assays of mouse fecal bacteria samples. L: mixed fecal bacteria  
900 samples collected from 3 mice with low levels of pre-existing S2 binding  
901 antibodies ( $OD_{450nm-630nm} \leq 0.140$  at serum dilution of 1:100); H: mixed fecal

902 bacteria samples collected from 3 mice with high levels of pre-existing S2  
903 binding antibodies ( $OD_{450nm-630nm} \geq 0.615$  at serum dilution of 1:100). **(B)** WB  
904 assays of fecal bacteria samples collected from 7 healthy individuals (Lanes  
905 1-7). All the mAbs and the control mouse IgG were diluted at the final  
906 concentration of 1 $\mu$ g/ml. Black arrows indicated the locations of protein bands  
907 chosen for the Mass spectrometry analysis.

908

909 **Figure 6 Impact of pre-existing antibodies on the humoral immune**  
910 **responses elicited by a DNA vaccine encoding SARS-CoV-2 S protein**

911 **(A)** Schematic illustration of the vaccination regimen. 50 $\mu$ g of the candidate  
912 DNA vaccine was injected intra muscularly into each mice at week 0, week 2  
913 and week 4. Two weeks after the final vaccination, the mice was sacrificed for  
914 the measurements of specific immune responses. **(B)** Peripheral blood was  
915 collected before immunization and levels of pre-existing S2 specific IgG were  
916 compared among three groups of mice. **(C)** Comparisons of endpoint IgG titers  
917 against S2 in the serum of mice measured at 2 weeks post the last  
918 immunization. **(D)** Comparisons of P144 specific IgG titers in the serum of  
919 mice as measured using BSA-P144 conjugate as the coating antigen. **(E)**  
920 Comparisons of P144 specific binding antibody levels as determined using a  
921 method of competitive ELISA. **(F)** Endpoint IgG titers against S1 measured at  
922 2 weeks post the final vaccination. **(G)** Neutralizing antibody titers against  
923 SARS-CoV-2 D614G pseudo-virus in serum of mice at 2 weeks post the final  
924 immunization. The vaccination experiment was repeated twice with 6 mice for  
925 each group. Data were shown as mean $\pm$ SD. Statistical analyses were  
926 performed by the method of one-way ANOVA.

927

928 **Figure 7 The impact of pre-existing antibody on the levels of specific IgG**  
929 **and IgA in BALF after vaccination**

930 BALF was collected from each mouse after euthanasia. Specific IgG (A and B)  
931 and IgA (C and D) against S1 or S2 were detected using in-house ELISA  
932 methods. All the BALF samples were adjusted to the initial total protein  
933 concentration of 51.9 $\mu$ g/ml. Data are shown as mean $\pm$  SD. Statistical analyses  
934 were performed by the method of one-way ANOVA.

935



936 **Figure 8 The impact of pre-existing antibody on the minimum epitope**  
937 **recognition of P144 after vaccination.**

938 The minimal epitope recognized by mouse sera after vaccination were  
939 analyzed using a method of competitive ELISA. Purified BSA-P144 conjugate  
940 was used as the coating antigen and truncated peptides derived from P144  
941 were used as the competitors. The decreases of competitive inhibition  
942 reflected the necessity of each amino acid for the epitope recognition.  
943 Statistical analyses were performed by the method of two-tailed t-test (\*,  $P <$   
944  $0.05$ , \*\*,  $P < 0.01$ , \*\*\*,  $P < 0.001$ ).

945

946 **Figure 9 The impact of pre-existing antibody on the cellular immune**  
947 **responses after vaccination**

948 (A) The diagram of the method for cellular immune responses assays. (B) S1  
949 and S2 specific IFN- $\gamma$  responses were compared among groups of mice with  
950 different levels of pre-existing S2 cross-reactive antibodies. Additionally, S1 (C)  
951 and S2 (D) specific releases of IL-2, IL-6 and TNF- $\alpha$  as measured using the  
952 method of multiplex cytokine bead assay were also compared among different  
953 groups. Data were shown as mean  $\pm$  SD. SFU, spot forming units.

954

955

956

957

958

959

960

961

962

963

964

965

966

967

968

969

970

971 **Supplementary figures**

972 **Supplementary Figure 1 A dominant linear epitope recognized by the**  
973 **pre-existing antibodies was located on the connector domain of S2**

974 (A) The location of P144 on the full length of SARS-CoV-2 spike protein.  
975 Synthesized peptides (18-mer, overlapped by 11 amino acids) spanning the full  
976 length of S2 were divided into 9 peptide pools, each contained 8 peptides. To  
977 identify the potential antibody binding epitopes, we first performed competitive  
978 ELISA assays using the peptide pools as competitors (Data not shown). The  
979 pool showing significant inhibition effect was further delineated by testing the  
980 inhibiting efficiencies of each individual peptides (B).

981 The data was shown as mean $\pm$ SD, n=5. Inhibition efficiencies among groups  
982 were analyzed using the method of One-way ANOVA. \*\*\*\*, p<0.0001. SP,  
983 signal peptide; RBD, receptor-binding domain; FP, fusion peptide; HR, heptad  
984 repeat; CH, central helix; CD, connector domain; TM, transmembrane domain;  
985 CT, cytoplasmic tail.

986

987 **Supplementary Figure 2 The pre-existing cross-reactive antibodies might**  
988 **be induced by exposure to certain gut microbial antigens**

989 (A) Principle component analysis (PCA) of gut microbial communities between  
990 4 mice in SPF condition and 4 mice in a sterile isolation pack. (B) The  
991 splenocytes and lymphocytes of MLN were harvested from 4 naive C57BL/6J  
992 mice with relatively high levels of pre-existing S2 cross-reactive antibodies. S2  
993 specific B cells were defined as CD45<sup>+</sup>CD19<sup>+</sup>S2<sup>+</sup> (Left). Statistical analysis  
994 was performed by the method of paired t-test (Right).

995

996 **Supplementary Figure 3 Characterizations of the minimal epitope**  
997 **recognitions for the 6 monoclonal antibodies isolated from naïve mice**

998 Six P144 specific monoclonal antibodies were isolated from 2 naïve SPF mice  
999 using the hybridoma technology. (A) The minimum epitope recognitions of  
1000 clones H9, E10, G13, F5 and G18 were similar detected by a method of  
1001 competitive ELISA. Purified S2 protein was used as the coating antigen and  
1002 the truncated peptides derived from P144 were used as the competitors. (B)  
1003 The epitope recognition of clone M3 was analyzed using purified S2 protein as  
1004 the coating antigen and each listed peptide was used as the competitor. SP,  
1005 signal peptide; RBD, receptor-binding domain; FP, fusion peptide; HR, heptad

1006 repeat; CH, central helix; CD, connector domain; TM, transmembrane domain;  
1007 CT, cytoplasmic tail.

1008

1009 **Supplementary Figure 4 Neutralizing activities of the purified monoclonal**  
1010 **antibodies as measured using a pseudo virus neutralization assay**

1011 Neutralization activities of 6 isolated mAbs against 5 major SARS-CoV-2  
1012 variants (D614G, B.1.617, B.1.1.7, B.1.351 and P.1) were examined using a  
1013 pseudo virus neutralization assay. Purified mouse IgG was used as negative  
1014 control and serum of an RBD protein vaccinated goat was use as positive  
1015 control. Purified mAbs and control mouse IgG were tested at a concentration  
1016 of 1µg/ml; positive goat serum was diluted at 1:90.

**Table 1** Demographics of SARS-CoV-2 unexposed healthy individuals

<b>Sample Collection Time</b>	<b>2016</b>	<b>2020</b>
Number of individuals	78	95
Gender (males, females)	17, 61	78, 17
Age, years (mean $\pm$ SD)	35.88 $\pm$ 8.40	30.40 $\pm$ 7.55

**Table 2** Potential cross-reactive antigens identified in mouse fecal bacteria

NCBI Accession #	Protein name	Bacterium	Score	Proteins	Unique Peptides	Peptides	PSMs	Area	MW [kDa]
Q8A470	DNA-directed RNA polymerase subunit beta' OS	Bacteroides thetaiotaomicron	168.01	550	2	6	6	3.536E7	158.3
Q5L897	DNA-directed RNA polymerase subunit beta OS	Bacteroides fragilis	92.15	8	2	3	3	8.315E6	142.4
Q8A1G1	TonB-dependent receptor SusC OS	Bacteroides thetaiotaomicron	145.74	1	1	2	3	1.385E8	111.1
Q46509	Aldehyde oxidoreductase OS	Desulfovibrio gigas	75.93	1	1	1	1	8.506E6	97.0
P22983	Pyruvate, phosphate dikinase OS	Clostridium symbiosum	109.83	7	2	2	2	3.721E7	96.6
P0A9Q8	Aldehyde-alcohol dehydrogenase OS	Escherichia coli	34.29	1	1	1	1	1.085E7	96.1
Q826F6	Chaperone protein dnaK2 OS	Streptomyces avermitilis	20.37	1	1	1	1	1.059E7	67.5
Q892R0	Chaperone protein DnaK OS	Clostridium tetani	51.52	5	1	1	1	1.780E7	66.4
B1I9W8	L-fucose isomerase OS	Streptococcus pneumoniae	57.33	12	2	2	2	2.792E7	65.7
P95334	Chaperone protein DnaK OS	Myxococcus xanthus	39.23	4	1	1	1	1.792E7	65.3
Q1MPZ9	Formate--tetrahydrofolate ligase OS	Lawsonia intracellularis	62.49	1	2	2	2	2.068E7	64.2
P26929	Urease subunit alpha OS	Lactobacillus fermentum	134.06	4	4	4	5	1.526E7	61.8
Q9I165	Periplasmic trehalase OS	Pseudomonas aeruginosa	77.05	1	1	1	1	4.240E8	61.1
Q9EZ02	Pyrophosphate--fructose 6-phosphate 1-phosphotransferase OS	Spirochaeta thermophila	68.21	2	1	1	1	1.192E7	61.0
P14407	Fumarate hydratase class I, anaerobic OS	Escherichia coli	30.79	1	1	1	1	6.580E6	60.1
Q189R2	Formate--tetrahydrofolate ligase OS	Clostridioides difficile	123.52	22	3	4	4	2.621E7	59.9
P22252	Flagellin B OS	Campylobacter jejuni subsp. jejuni serotype O:6	75.42	1	1	1	1	1.478E7	59.7
Q1WTW0	Formate--tetrahydrofolate ligase OS	Lactobacillus salivarius	83.43	23	1	1	1	5.229E7	59.4
A7HLZ4	Formate--tetrahydrofolate ligase OS	Fervidobacterium nodosum	93.49	29	1	2	2	8.036E6	59.2
C4ZBL1	Phosphoenolpyruvate carboxykinase (ATP) OS	Agathobacter rectalis	211.34	4	1	4	5	3.965E7	59.0
A6LFQ4	Phosphoenolpyruvate carboxykinase (ATP) OS	Parabacteroides distasonis	32.29	1	1	1	1	8.523E6	58.9
A3MZI4	Formate--tetrahydrofolate ligase OS	Actinobacillus pleuropneumoniae serotype 5b	78.45	78	1	2	2	1.320E8	58.9
Q2LPJ8	60 kDa chaperonin 1 OS	Syntrophus aciditrophicus	101.22	15	1	2	3	2.217E7	58.6
Q3ALZ3	60 kDa chaperonin 1 OS	Synechococcus sp.	113.34	23	1	2	3	9.973E7	58.5
B8J123	60 kDa chaperonin OS	Desulfovibrio desulfuricans	232.59	27	2	5	6	9.659E7	58.4
Q72AL6	60 kDa chaperonin OS	Desulfovibrio vulgaris	126.02	9	1	3	3	2.402E7	58.4

A0Q2T1	60 kDa chaperonin OS	<i>Clostridium novyi</i>	78.78	16	1	2	2	2.292E7	58.1
B0SCC0	60 kDa chaperonin OS	<i>Leptospira biflexa</i> serovar Patoc	49.58	1	1	1	1	1.882E8	58.1
B2TIX0	60 kDa chaperonin OS	<i>Clostridium botulinum</i>	126.34	35	1	3	3	4.903E7	57.9
A7GZ43	60 kDa chaperonin OS	<i>Campylobacter curvus</i>	105.05	41	2	3	3	5.327E7	57.9
Q67KB8	60 kDa chaperonin OS	<i>Symbiobacterium thermophilum</i>	107.47	126	1	3	3	9.411E7	57.9
B5YDR9	60 kDa chaperonin OS	<i>Dictyoglomus thermophilum</i>	59.61	2	1	1	1	3.345E7	57.9
Q3ADX3	60 kDa chaperonin OS	<i>Carboxydotherrnus hydrogenoformans</i>	104.07	25	1	2	3	7.715E7	57.6
O50305	60 kDa chaperonin OS	<i>Bacillus halodurans</i>	250.57	55	3	4	6	3.021E8	57.4
P26821	60 kDa chaperonin OS	<i>Clostridium perfringens</i>	131.27	36	1	3	3	4.609E7	57.3
P37282	60 kDa chaperonin OS	<i>Lactococcus lactis</i> subsp. <i>lactis</i>	102.15	18	1	2	2	4.298E7	57.2
C4ZD46	60 kDa chaperonin OS	<i>Agathobacter rectalis</i>	372.10	52	3	5	8	3.352E8	57.1
A6L8C4	Glucose-6-phosphate isomerase OS	<i>Parabacteroides distasonis</i>	88.85	55	1	2	3	5.392E8	48.7
P43793	NADP-specific glutamate dehydrogenase OS	<i>Haemophilus influenzae</i>	96.32	2	1	2	2	7.357E7	48.6
P00370	NADP-specific glutamate dehydrogenase OS	<i>Escherichia coli</i>	161.88	1	1	3	4	3.280E8	48.6
P15111	NADP-specific glutamate dehydrogenase OS	<i>Salmonella typhimurium</i>	185.28	4	1	4	5	1.755E8	48.5
P94316	NAD-specific glutamate dehydrogenase OS	<i>Bacteroides fragilis</i>	192.93	3	3	5	6	1.730E8	48.4
Q1WSY0	Enolase OS	<i>Lactobacillus salivarius</i>	79.89	8	3	3	3	1.340E7	48.0
B7MD95	Trigger factor OS	<i>Escherichia coli</i> O45:K1	78.80	10	2	2	2	4.344E7	47.8
B2GAM0	Enolase OS	<i>Lactobacillus fermentum</i>	79.94	8	2	2	2	1.858E7	47.8
Q6MEY2	Enolase OS	<i>Protochlamydia amoebophila</i>	112.67	1	1	1	1	7.493E7	47.5
Q0SNH5	Enolase OS	<i>Borrelia afzelii</i>	71.86	2	1	1	1	4.654E7	47.4
G3KIM4	Lactoyl-CoA dehydratase subunit alpha (Fragment) OS	<i>Anaerotignum propionicum</i>	63.03	1	1	1	1	1.136E7	47.4
Q9I3S1	Biofilm dispersion protein BdlA OS	<i>Pseudomonas aeruginosa</i>	59.07	22	1	1	1	3.282E7	46.9
B8J4A8	Sulfate adenyllyltransferase OS	<i>Desulfovibrio desulfuricans</i>	210.65	1	5	5	5	2.656E7	46.9
A6L3M9	Enolase OS	<i>Bacteroides vulgatus</i>	48.62	2	1	2	2	3.004E7	46.7
Q043Z5	Enolase 1 OS	<i>Lactobacillus gasseri</i>	289.72	4	5	5	5	4.189E7	46.6
Q1ISS7	Enolase OS	<i>Koribacter versatilis</i>	71.57	4	1	1	1	7.884E6	46.5
B8DTI9	Enolase OS	<i>Bifidobacterium animalis</i> subsp. <i>lactis</i>	115.71	4	2	2	2	1.684E7	46.4
A7GUR7	Enolase OS	<i>Bacillus cytotoxicus</i>	122.68	17	2	2	3	2.771E7	46.4
Q2LR33	Enolase OS	<i>Syntrophus aciditrophicus</i>	31.73	1	1	1	1	4.823E7	46.2
Q89Z05	Enolase OS	<i>Bacteroides thetaiotaomicron</i>	140.16	2	2	4	5	3.005E7	46.1



B2RLL7	Enolase OS	Porphyromonas gingivalis	123.91	2	2	3	3	2.636E7	45.8
Q6MPQ2	Enolase OS	Bdellovibrio bacteriovorus	66.50	1	1	1	1	8.918E6	45.7
B0K742	Serine hydroxymethyltransferase OS	Thermoanaerobacter pseudethanolicus	85.67	92	2	2	2	2.140E7	45.6
Q5LFT7	Peptidase T OS	Bacteroides fragilis	89.56	5	1	1	1	7.323E7	45.5
A9NEA9	Serine hydroxymethyltransferase OS	Acholeplasma laidlawii	44.82	3	1	1	1	5.875E6	45.3
Q7MU77	Phosphoglycerate kinase OS	Porphyromonas gingivalis	54.70	1	1	1	1	2.106E7	45.0
Q8A753	Phosphoglycerate kinase OS	Bacteroides thetaiotaomicron	25.30	1	1	1	1	1.320E7	45.0
A5VHR0	Phosphopentomutase OS	Lactobacillus reuteri	159.08	1	4	4	4	4.364E7	44.0
A8EWM4	Phosphoglycerate kinase OS	Arcobacter butzleri	45.52	1	1	1	1	2.577E7	43.8
Q042T5	Elongation factor Tu OS	Lactobacillus gasseri	400.92	36	3	10	13	1.184E8	43.7
Q74JU6	Elongation factor Tu OS	Lactobacillus johnsonii	348.06	36	2	9	12	1.184E8	43.6
Q5L890	Elongation factor Tu OS	Bacteroides fragilis	185.88	297	3	5	7	1.454E8	43.6
Q8R603	Elongation factor Tu OS	Fusobacterium nucleatum subsp. nucleatum	150.02	302	1	3	3	6.170E7	43.4
B8J1A0	Elongation factor Tu OS	Desulfovibrio desulfuricans	139.50	64	2	3	3	4.287E7	43.4
A5VJ92	Elongation factor Tu OS	Lactobacillus reuteri	413.79	60	8	11	13	3.595E8	43.4

**Note:** *Score:* The Mascot score. *Proteins:* The total number of proteins contained in the protein group. *Unique Peptides:* The total number of peptides unique to the protein group. *Peptides:* The total number of peptides identified from all included searches for the master protein of the protein group. *PSMs:* The total number of peptide-spectrum matches identified from all included searches for the master protein of the protein group. *Area:* The chromatographic peak area was used to characterize the quantitative abundance of protein. *MW(kDa):* The theoretical molecular weight of the protein.

**Table 3** Potential cross-reactive antigens identified in human fecal bacteria

NCBI Accession #	Protein Name	Bacterium	Score	Proteins	Unique Peptides	Peptides	PSMs	Area	MW [kDa]
A6LFK9	Polyribonucleotide nucleotidyltransferase OS	Parabacteroides distasonis	62.68	3	1	2	2	2.332E7	82.0
P75764	Uncharacterized protein YbhJ OS	Escherichia coli	27.35	1	1	1	1	3.198E7	81.5
Q8A4N6	Polyribonucleotide nucleotidyltransferase OS	Bacteroides thetaiotaomicron	226.97	23	6	7	7	6.947E7	78.3
B3DT30	Elongation factor G OS	Bifidobacterium longum	236.98	64	8	10	11	4.407E7	78.1
E1WNR6	Chaperone protein htpG OS	Bacteroides fragilis	131.15	4	1	2	2	4.992E7	77.9
O31673	ATP-dependent Clp protease ATP-binding subunit ClpE OS	Bacillus subtilis	120.19	73	1	3	4	8.448E7	77.9
A7ZSL5	Elongation factor G OS	Escherichia coli O139:H28	133.81	92	2	3	4	2.888E7	77.5
Q5L8A7	Elongation factor G OS	Bacteroides fragilis	431.35	187	3	10	14	1.391E8	77.5
A6KYJ7	Elongation factor G OS	Bacteroides vulgatus	361.61	186	2	9	12	1.342E8	77.4
A6LFP0	Methionine--tRNA ligase OS	Parabacteroides distasonis	65.86	8	1	1	1	4.772E7	77.4
A3PV95	Elongation factor G OS	Mycobacterium sp.	134.99	70	1	4	5	1.255E8	77.3
P39396	Pyruvate/proton symporter BtsT OS	Escherichia coli	92.20	1	2	2	2	1.446E7	77.3
A9KNK6	Polyribonucleotide nucleotidyltransferase OS	Lachnoclostridium phytofermentans	68.87	1	1	1	1	1.075E8	76.9
Q5L6S5	Elongation factor G OS	Chlamydia abortus	76.05	58	1	2	3	1.622E7	76.8
Q67JU0	Elongation factor G OS	Symbiobacterium thermophilum	147.39	86	1	4	5	2.631E8	76.8
Q5U8S9	Elongation factor G OS	Staphylococcus intermedius	98.88	65	1	3	4	5.177E7	76.7
Q8A294	Putative K(+)-stimulated pyrophosphate-energized sodium pump OS	Bacteroides thetaiotaomicron	150.65	20	1	3	3	1.276E8	76.5
B9DYA6	Elongation factor G OS	Clostridium kluyveri	136.00	67	1	3	4	8.826E7	76.4
Q5WLR5	Elongation factor G OS	Bacillus clausii	134.85	81	1	4	5	1.119E8	76.4
Q97I51	Translation initiation factor IF-2 OS	Clostridium acetobutylicum	70.53	4	1	1	1	2.330E8	76.3
A0PXU3	Elongation factor G OS	Clostridium novyi	114.21	67	1	3	4	8.905E7	76.1
Q18CF4	Elongation factor G OS	Clostridioides difficile	174.49	59	1	4	5	1.288E8	75.8
Q8AB53	Putative glucosamine-6-phosphate deaminase-like protein BT_0258 OS	Bacteroides thetaiotaomicron	54.10	1	1	1	1	4.629E6	75.2
Q8XJ01	Penicillin-binding protein 1A OS	Clostridium perfringens	39.66	3	1	1	1	1.599E7	75.1
A6L7J7	Threonine--tRNA ligase OS	Bacteroides vulgatus	91.33	9	2	2	2	2.440E7	74.2
P30539	1,4-alpha-glucan branching enzyme GlgB OS	Butyrivibrio fibrisolvens	30.12	1	1	1	1	2.287E7	73.8

B2TIT5	Threonine--tRNA ligase OS	Clostridium botulinum	53.61	2	1	1	1	1.877E7	73.8
P56116	Chaperone protein HtpG OS	Helicobacter pylori	38.02	12	1	1	1	1.269E7	71.2
P0A9P7	ATP-dependent RNA helicase DeaD OS	Escherichia coli O6:H1	85.88	5	3	3	4	1.336E8	70.5
P19410	3-oxocholoyl-CoA 4-desaturase OS	Clostridium scindens	63.87	1	1	1	1	5.844E7	70.2
O53182	2-oxoglutarate oxidoreductase subunit KorA OS	Mycobacterium tuberculosis	67.48	1	1	1	1	3.826E7	69.1
Q8RHJ2	Putative K(+)-stimulated pyrophosphate-energized sodium pump OS	Fusobacterium nucleatum subsp. nucleatum	140.41	23	1	3	3	1.320E8	68.9
A5CX56	Chaperone protein DnaK OS	Vesicomysocius okutanii subsp. Calyptogena okutanii	15.38	1	1	1	1	2.961E7	68.7
Q5LG30	Chaperone protein DnaK OS	Bacteroides fragilis	418.39	33	1	9	11	6.399E7	68.6
Q89YW6	Chaperone protein DnaK OS	Bacteroides thetaiotaomicron	372.24	35	1	7	9	6.399E7	68.3
A6L2X7	Chaperone protein DnaK OS	Bacteroides vulgatus	371.71	33	1	8	10	6.399E7	68.3
Q93GF1	Chaperone protein DnaK OS	Prevotella loescheii	185.46	1	4	4	4	3.512E7	68.0
A6LGR5	4-hydroxy-3-methylbut-2-en-1-yl diphosphate synthase (flavodoxin) OS	Parabacteroides distasonis	38.34	5	1	1	1	2.396E7	67.9
B8H444	ATP-dependent zinc metalloprotease FtsH OS	Caulobacter vibrioides	26.45	6	1	1	1	1.241E7	67.7
A9KIA6	Aspartate--tRNA(Asp/Asn) ligase OS	Lachnoclostridium phytofermentans	31.12	1	1	1	1	8.400E6	67.5
P0AG91	Protein translocase subunit SecD OS	Escherichia coli O157:H7	233.70	2	6	6	6	2.164E7	66.6
Q49Y22	Chaperone protein DnaK OS	Staphylococcus saprophyticus subsp. saprophyticus	56.64	206	1	2	2	1.171E7	66.5
A6LBU6	Aspartate--tRNA ligase OS	Parabacteroides distasonis	88.06	49	1	2	2	7.901E6	66.4
P21332	Oligo-1,6-glucosidase OS	Bacillus cereus	53.99	2	1	1	1	1.391E7	66.0
Q8A5W4	Lysine--tRNA ligase OS	Bacteroides thetaiotaomicron	154.84	2	2	2	2	1.304E7	65.9
Q8GBW6	Methylmalonyl-CoA carboxyltransferase 12S subunit OS	Propionibacterium freudenreichii subsp. shermanii	98.01	1	1	1	2	1.386E8	65.9
Q67S54	Chaperone protein DnaK OS	Symbiobacterium thermophilum	96.29	225	1	3	3	4.528E7	65.7
Q9RQ13	L-fucose isomerase OS	Bacteroides thetaiotaomicron	181.20	7	1	5	7	1.038E8	65.7
A6L048	L-fucose isomerase OS	Bacteroides vulgatus	162.35	5	2	6	7	3.672E7	65.6
Q56403	V-type ATP synthase alpha chain OS	Thermus thermophilus	132.50	30	1	1	2	1.117E7	63.6
Q8G716	Glucose-6-phosphate isomerase OS	Bifidobacterium longum	531.07	4	14	14	15	3.155E8	63.0
Q4JX51	Glucose-6-phosphate isomerase OS	Corynebacterium jeikeium	30.85	1	1	1	1	3.306E7	62.1
Q8FZC4	2-isopropylmalate synthase OS	Brucella suis biovar 1	51.65	8	1	1	1	1.014E7	61.6

A6TGT4	Glucose-6-phosphate isomerase OS	Klebsiella pneumoniae subsp. pneumoniae	53.60	21	1	1	1	3.337E7	61.3
P0AG69	30S ribosomal protein S1 OS	Escherichia coli O157:H7	88.52	1	2	2	2	8.393E6	61.1
Q9EZ02	Pyrophosphate--fructose 6-phosphate 1-phosphotransferase OS	Spirochaeta thermophila	110.07	2	2	2	2	1.245E8	61.0
O31716	Uncharacterized ABC transporter ATP-binding protein YkpA OS	Bacillus subtilis	48.45	1	1	1	1	2.259E6	61.0
P59173	Probable 2,3-bisphosphoglycerate-independent phosphoglycerate mutase OS	Leptospira interrogans serogroup Icterohaemorrhagiae serovar Lai	61.50	2	1	1	2	6.104E6	61.0
P23843	Periplasmic oligopeptide-binding protein OS	Escherichia coli	368.94	2	11	11	12	1.586E8	60.9
Q0SQ82	Formate--tetrahydrofolate ligase OS	Clostridium perfringens	167.47	26	1	3	4	6.063E7	60.4
P14407	Fumarate hydratase class I, anaerobic OS	Escherichia coli	66.46	4	2	2	2	4.922E7	60.1
Q3A9K2	Formate--tetrahydrofolate ligase OS	Carboxydotherrmus hydrogenoformans	110.68	55	1	3	3	3.356E8	60.1
Q251P8	Formate--tetrahydrofolate ligase 1 OS	Desulfitobacterium hafniense	72.85	55	1	2	2	5.742E8	60.0
C0QX38	Formate--tetrahydrofolate ligase OS	Brachyspira hyodysenteriae	145.04	9	1	2	3	2.562E7	60.0
Q189R2	Formate--tetrahydrofolate ligase OS	Clostridioides difficile	157.46	1	3	3	3	1.347E9	59.9
C4ZBG8	Formate--tetrahydrofolate ligase OS	Agathobacter rectalis	235.86	56	4	6	6	3.610E8	59.7
A8AQV7	Phosphoenolpyruvate carboxykinase (ATP) OS	Citrobacter koseri	104.30	44	4	5	5	1.300E8	59.6
Q24ZZ8	Formate--tetrahydrofolate ligase 2 OS	Desulfitobacterium hafniense	79.67	55	1	2	2	5.193E8	59.4
B2RHV8	Phosphoenolpyruvate carboxykinase (ATP) OS	Porphyromonas gingivalis	188.39	21	2	5	5	2.446E8	59.4
Q47VD0	Phosphoenolpyruvate carboxykinase (ATP) OS	Colwellia psychrerythraea	111.53	16	1	2	2	1.952E8	59.3
P9WQH6	Probable propionyl-CoA carboxylase beta chain 5 OS	Mycobacterium tuberculosis	59.03	2	1	1	1	5.556E7	59.3
A1R7X2	Arginine--tRNA ligase OS	Paenarthrobacter aurescens	43.93	15	1	1	1	2.994E7	59.2
Q8A414	Phosphoenolpyruvate carboxykinase (ATP) OS	Bacteroides thetaiotaomicron	293.03	21	3	8	8	3.939E8	59.1
C4ZBL1	Phosphoenolpyruvate carboxykinase (ATP) OS	Agathobacter rectalis	501.52	17	5	12	15	4.167E8	59.0
Q5L7N5	Phosphoenolpyruvate carboxykinase (ATP) OS	Bacteroides fragilis	420.91	17	1	6	12	2.103E8	59.0
A3CL27	Formate--tetrahydrofolate ligase 1 OS	Streptococcus sanguinis	145.32	20	1	2	3	3.296E7	59.0
A6LFQ4	Phosphoenolpyruvate carboxykinase (ATP) OS	Parabacteroides distasonis	438.19	17	5	11	14	2.336E8	58.9
C4ZAW6	Dihydroxy-acid dehydratase OS	Agathobacter rectalis	193.87	6	5	6	6	2.765E7	58.9
B9E299	Dihydroxy-acid dehydratase OS	Clostridium kluyveri	85.82	2	1	2	3	7.244E7	58.8
O09460	Phosphoenolpyruvate carboxykinase (ATP) OS	Anaerobiospirillum succiniciproducens	214.42	21	2	5	5	3.702E8	58.6
B2TIR2	Dihydroxy-acid dehydratase OS	Clostridium botulinum	46.21	2	1	1	1	3.131E6	58.5

B3DTV2	ATP synthase subunit alpha OS	Bifidobacterium longum	383.31	393	9	11	12	5.746E7	58.4
B3DRY6	Bifunctional purine biosynthesis protein PurH OS	Bifidobacterium longum	204.27	2	3	3	3	1.243E8	58.4
A6LIG0	60 kDa chaperonin OS	Parabacteroides distasonis	325.96	2	1	7	10	4.117E8	58.3
A5N857	Ribonuclease Y OS	Clostridium kluyveri	85.68	95	1	3	3	4.874E7	58.3
Q8G3N6	Inosine-5'-monophosphate dehydrogenase OS	Bifidobacterium longum	685.57	20	15	16	19	2.005E8	58.2
Q8A6P8	60 kDa chaperonin OS	Bacteroides thetaiotaomicron	591.81	1	2	11	15	2.794E8	58.2
Q5LAF6	60 kDa chaperonin OS	Bacteroides fragilis	690.75	1	4	15	20	5.301E8	58.2
A0Q2T1	60 kDa chaperonin OS	Clostridium novyi	58.42	6	2	2	2	2.212E8	58.1
A6KXA0	60 kDa chaperonin OS	Bacteroides vulgatus	948.24	1	11	22	26	6.146E8	58.1

**Note:** *Score:* The Mascot score. *Proteins:* The total number of proteins contained in the protein group. *Unique Peptides:* The total number of peptides unique to the protein group. *Peptides:* The total number of peptides identified from all included searches for the master protein of the protein group. *PSMs:* The total number of peptide-spectrum matches identified from all included searches for the master protein of the protein group. *Area:* The chromatographic peak area was used to characterize the quantitative abundance of protein. *MW(kDa):* The theoretical molecular weight of the protein.

# Figure 1 Pre-existing cross-reactive antibodies against SARS-CoV-2 S protein observed in both healthy human and naive SPF mice predominantly targeted S2 subunit

medRxiv preprint doi: <https://doi.org/10.1101/2021.07.13.21260404>; this version posted July 15, 2021. The copyright holder for this preprint (which was not certified by peer review) is the author/funder, who has granted medRxiv a license to display the preprint in perpetuity. All rights reserved. No reuse allowed without permission.

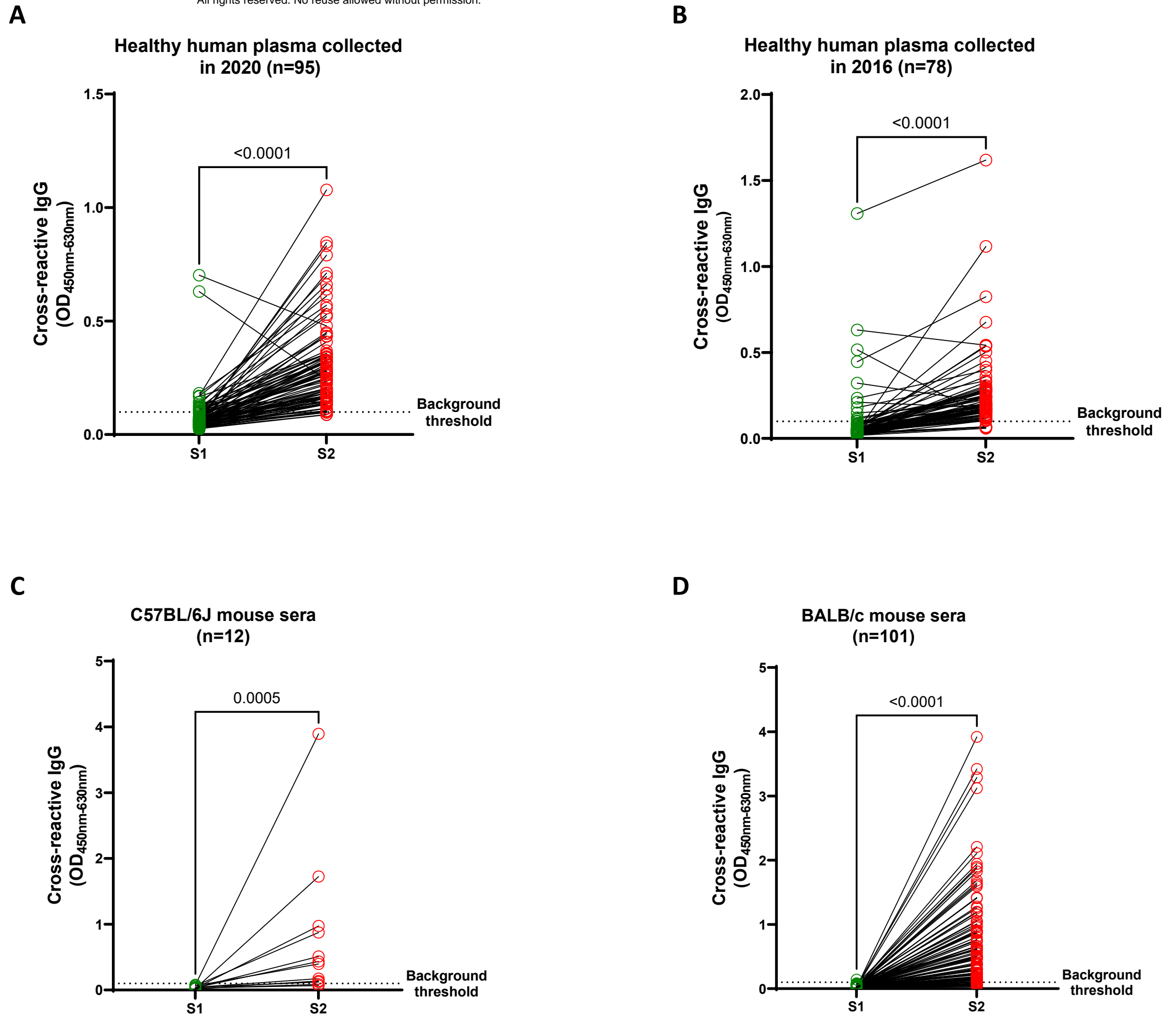




**Figure 2** The pre-existing S protein cross-reactive antibodies in naïve SPF mice recognized S2 exclusively and a dominant linear antibody epitope was identified on the connector domain

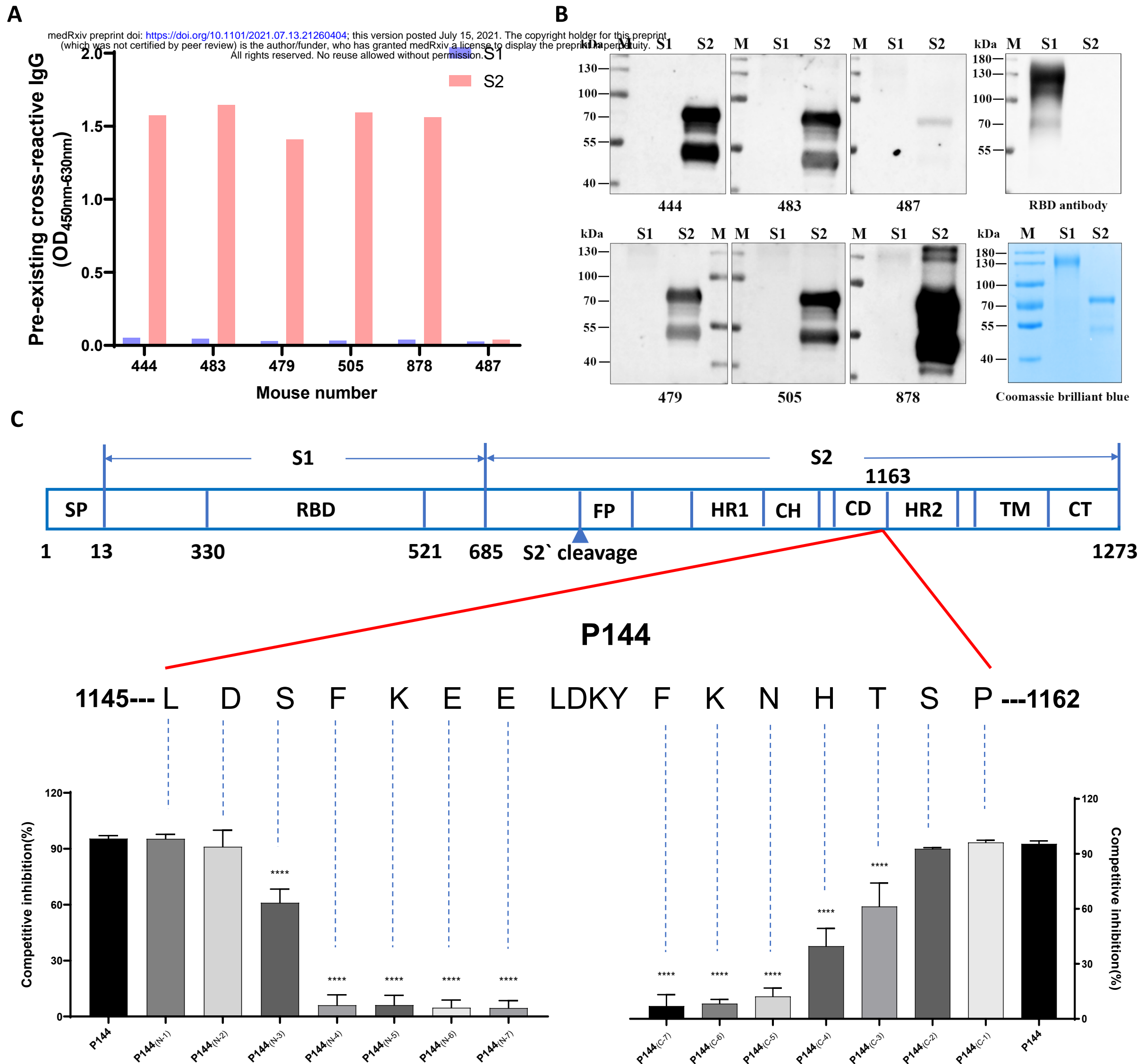


# Figure 3 Cross-reactive antibodies recognizing epitope P144 widely existed in both healthy human and naïve SPF mice

medRxiv preprint doi: <https://doi.org/10.1101/2021.07.13.21260404>; this version posted July 15, 2021. The copyright holder for this preprint (which was not certified by peer review) is the author/funder, who has granted medRxiv a license to display the preprint in perpetuity. All rights reserved. No reuse allowed without permission.

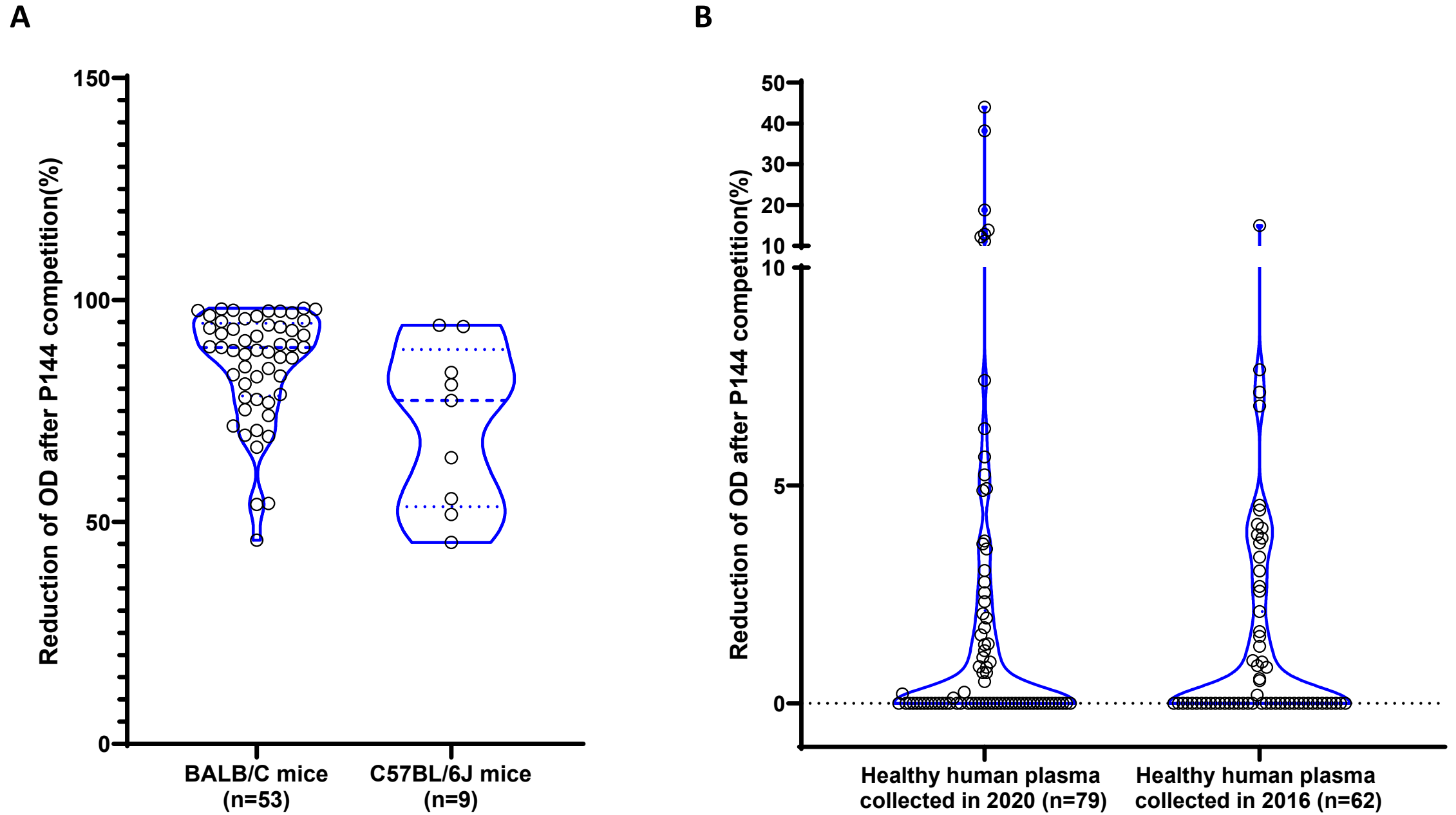
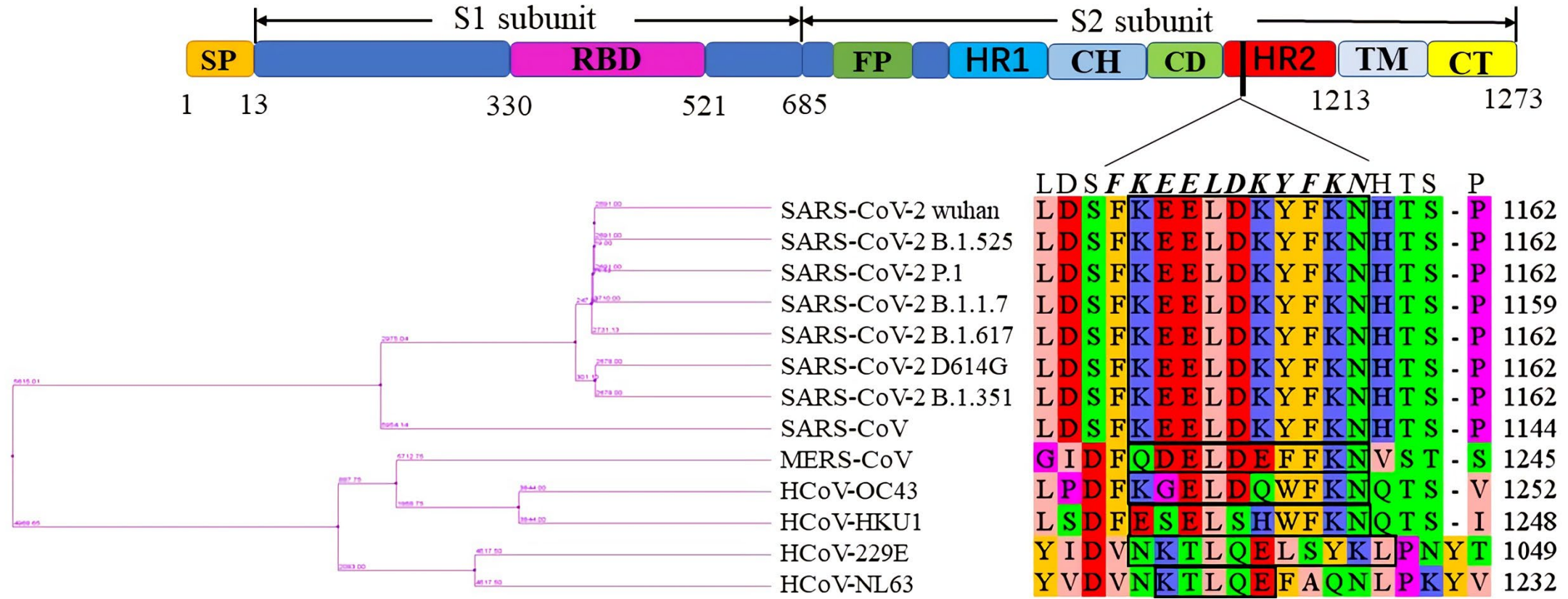


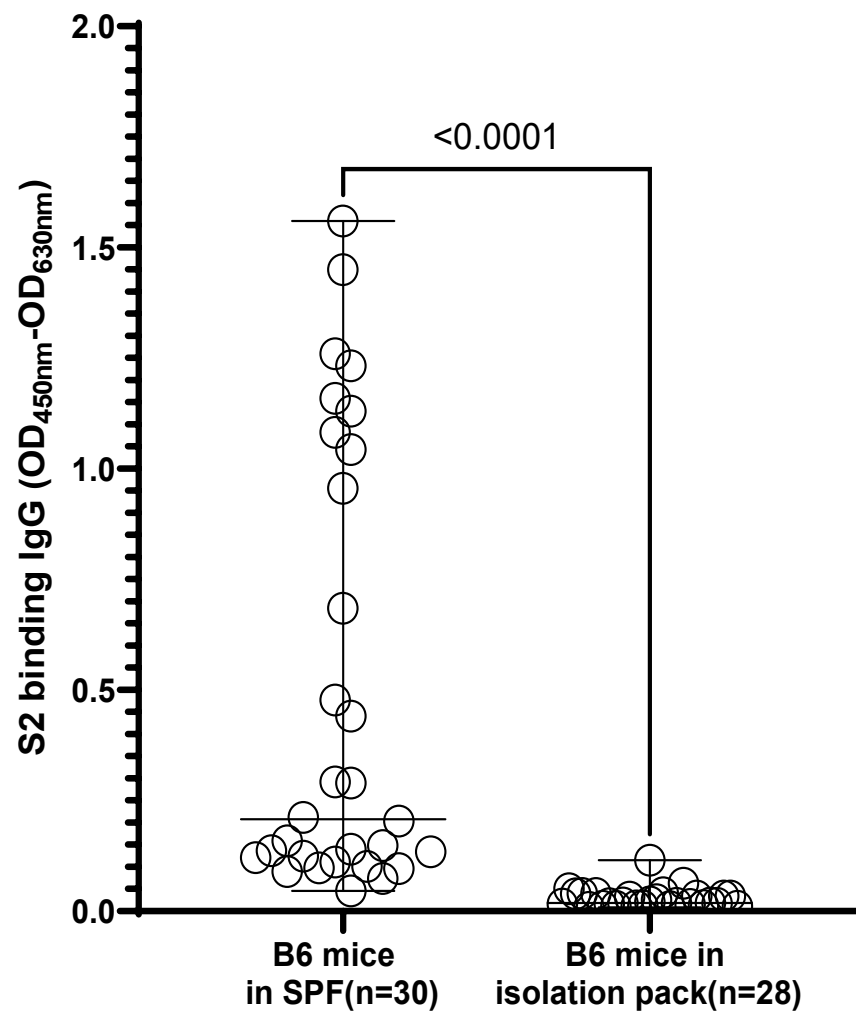
# Figure 4 The generation of the pre-existing S2 cross-reactive antibodies might be associated with commensal gut microbiota

**A**

medRxiv preprint doi: <https://doi.org/10.1101/2021.07.13.21260404>; this version posted July 15, 2021. The copyright holder for this preprint (which was not certified by peer review) is the author/funder, who has granted medRxiv a license to display the preprint in perpetuity. All rights reserved. No reuse allowed without permission.



**B**



**C**

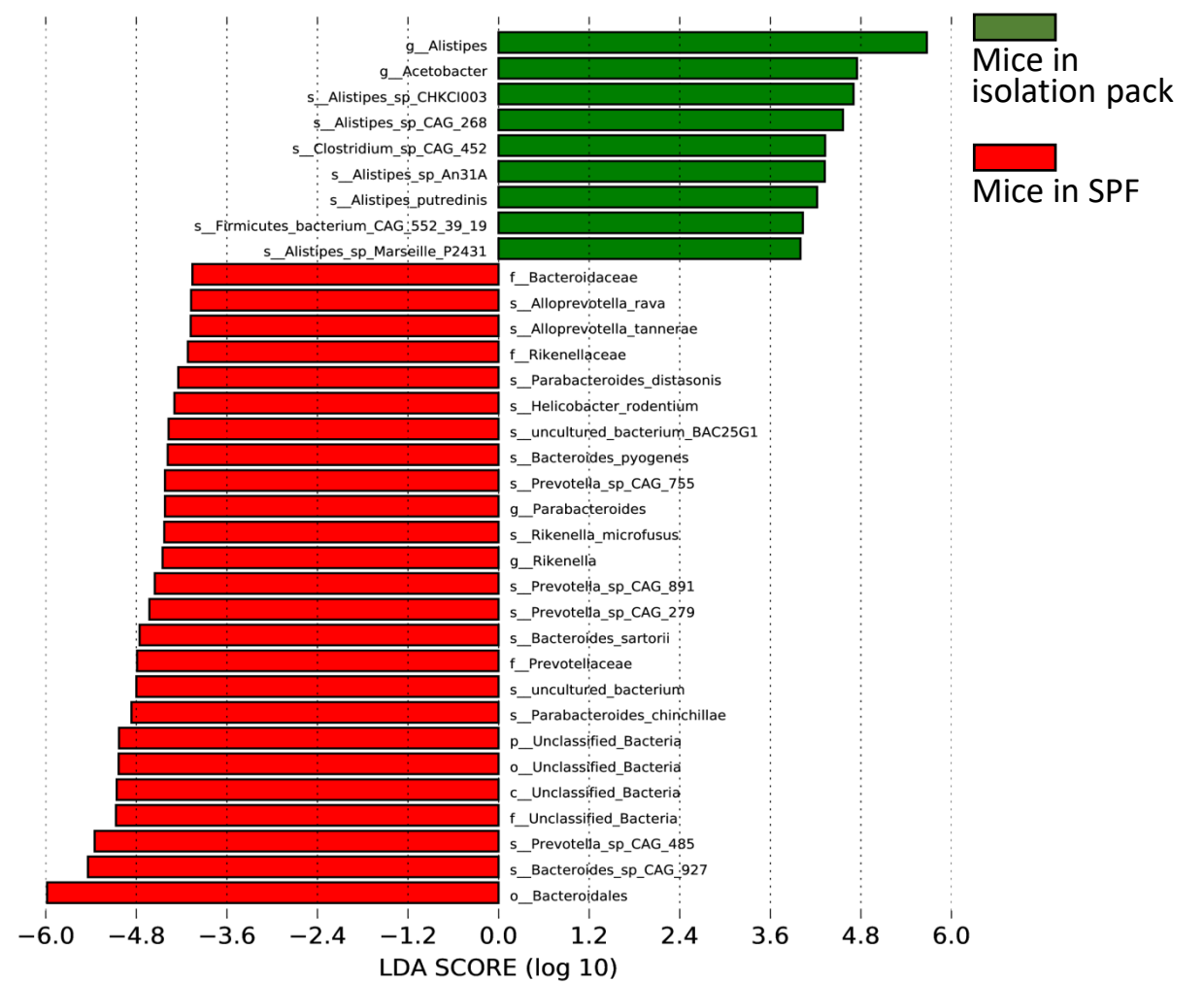


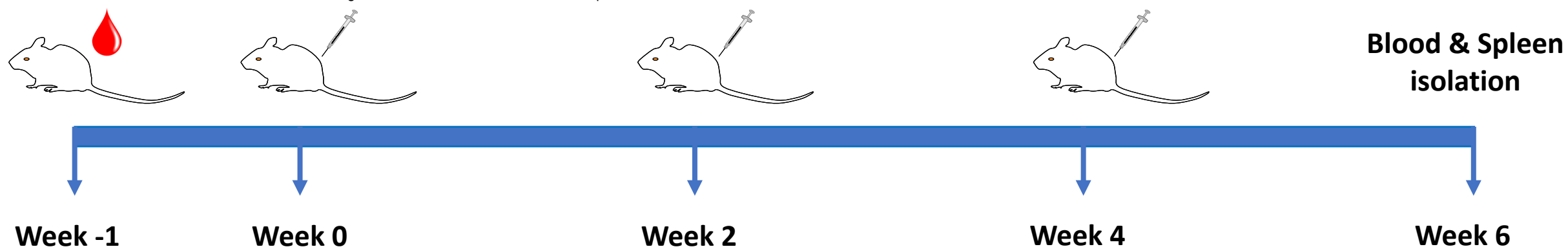




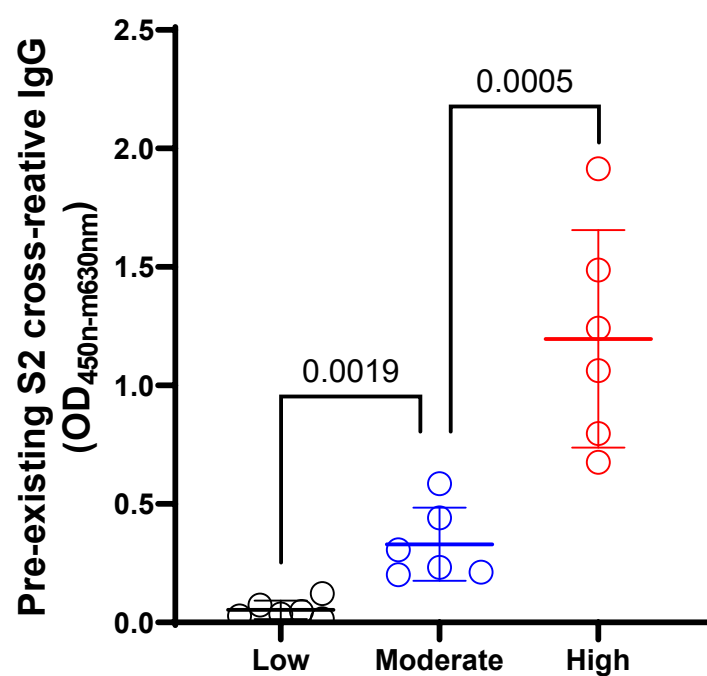
# Figure 6 The impact of pre-existing antibody on the humoral immune responses elicited by a DNA vaccine encoding SARS-CoV-2 S protein

medRxiv preprint doi: <https://doi.org/10.1101/2021.07.13.21260404>; this version posted July 15, 2021. The copyright holder for this preprint (which was not certified by peer review) is the author/funder, who has granted medRxiv a license to display the preprint in perpetuity. All rights reserved. No reuse allowed without permission.

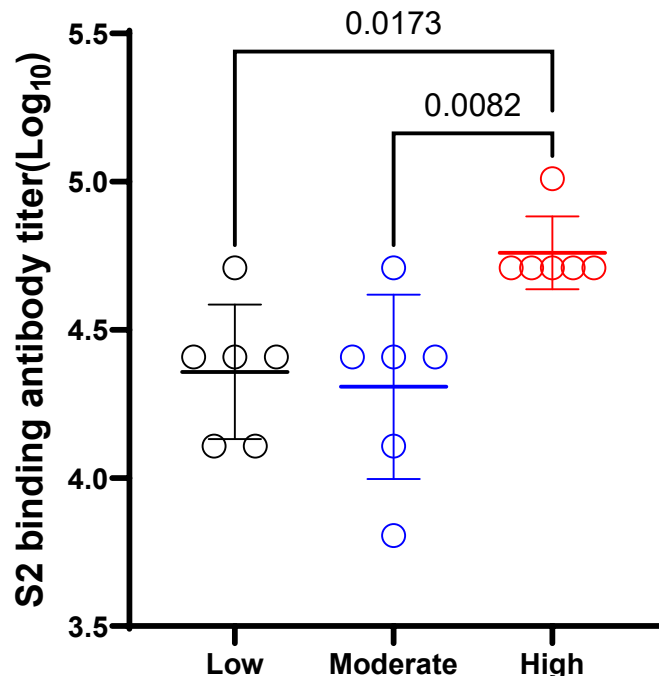
**A**



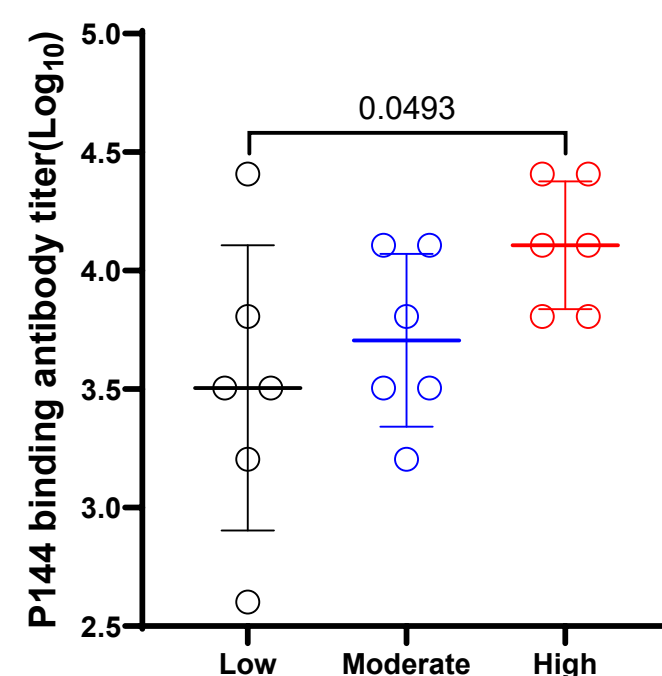
**B**



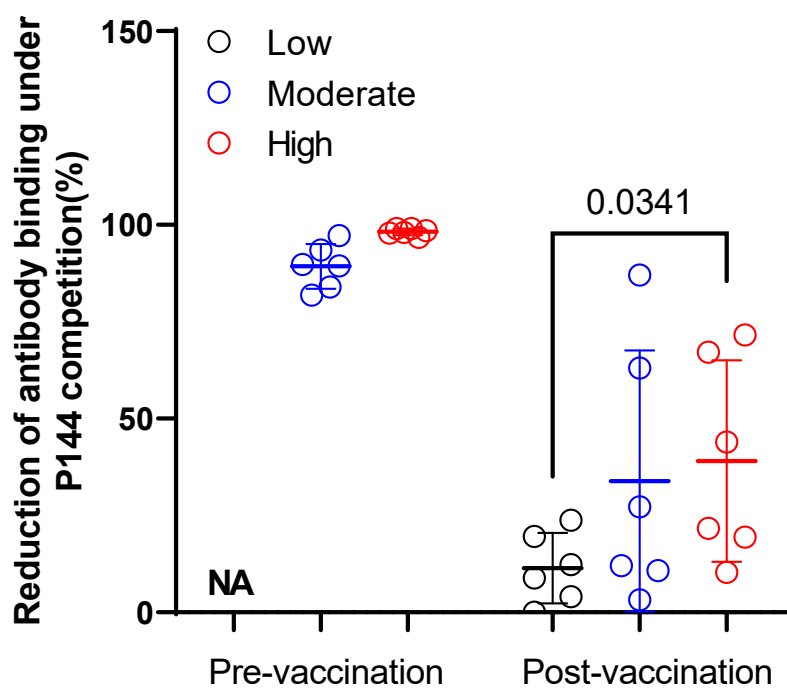
**C**



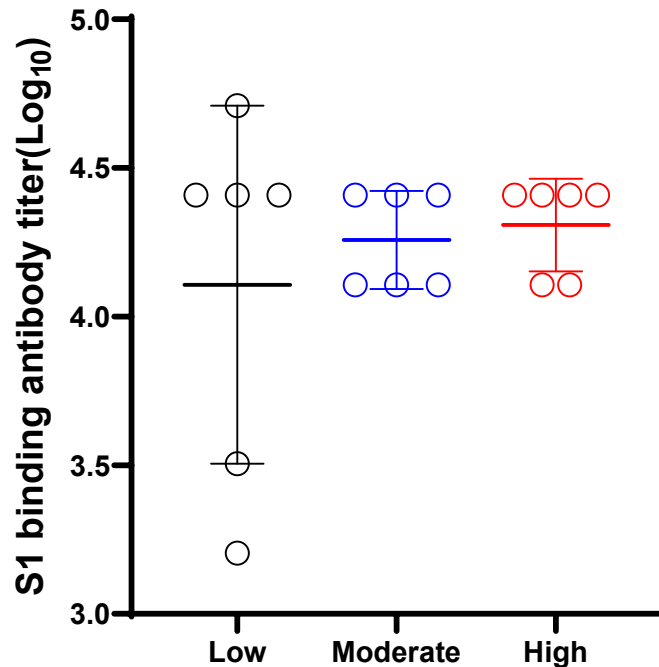
**D**



**E**



**F**



**G**

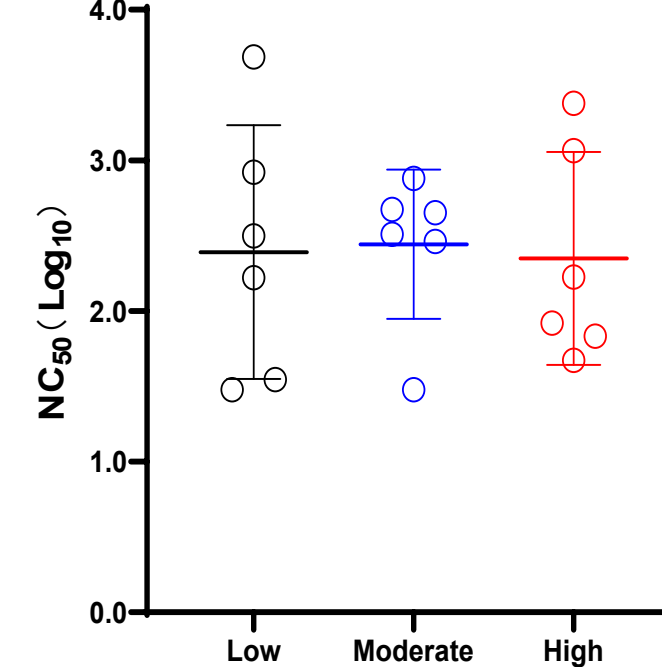
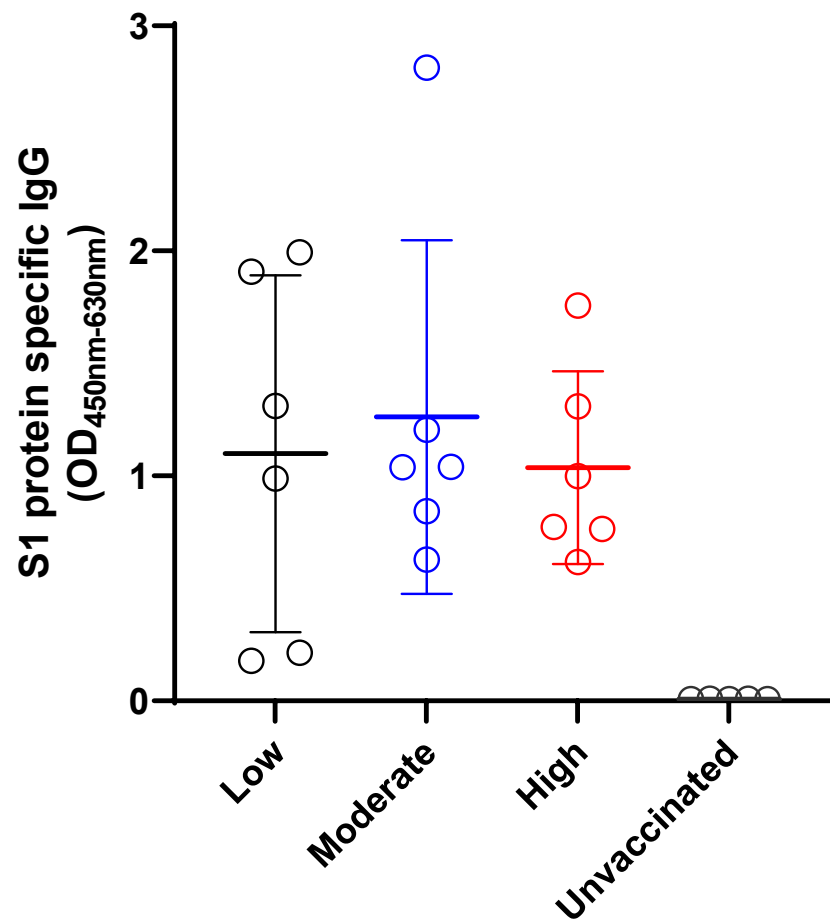


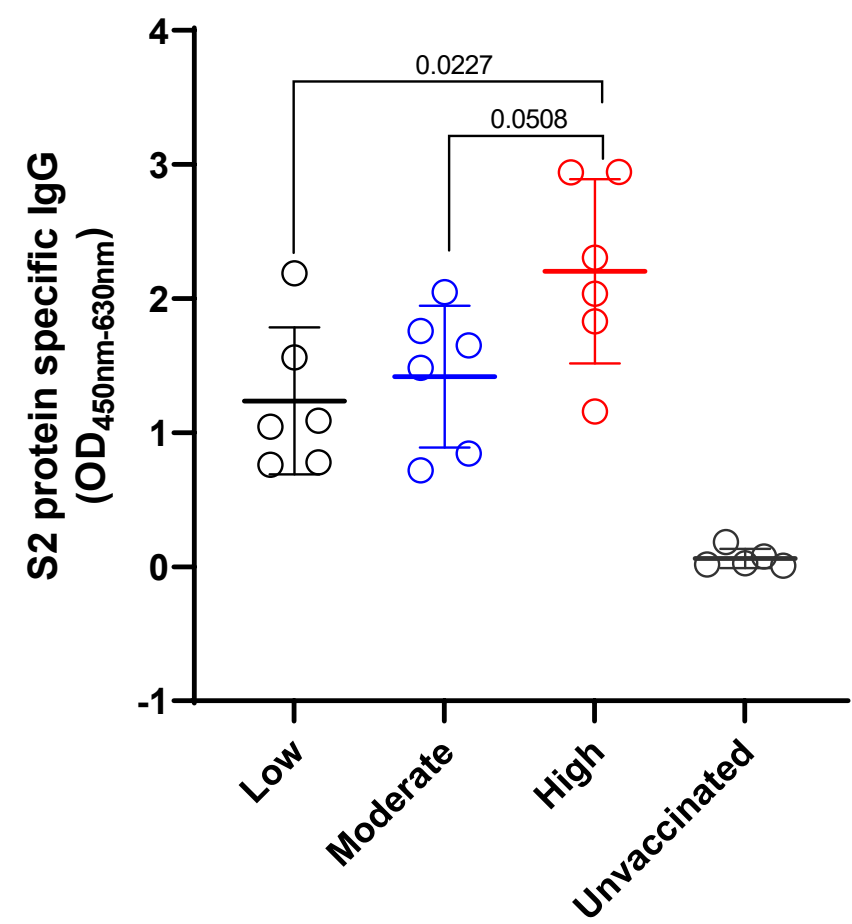
# Figure 7 The impact of pre-existing antibody on the levels of specific IgG and IgA in BALF after vaccination

medRxiv preprint doi: <https://doi.org/10.1101/2021.07.13.21260404>; this version posted July 15, 2021. The copyright holder for this preprint (which was not certified by peer review) is the author/funder, who has granted medRxiv a license to display the preprint in perpetuity. All rights reserved. No reuse allowed without permission.

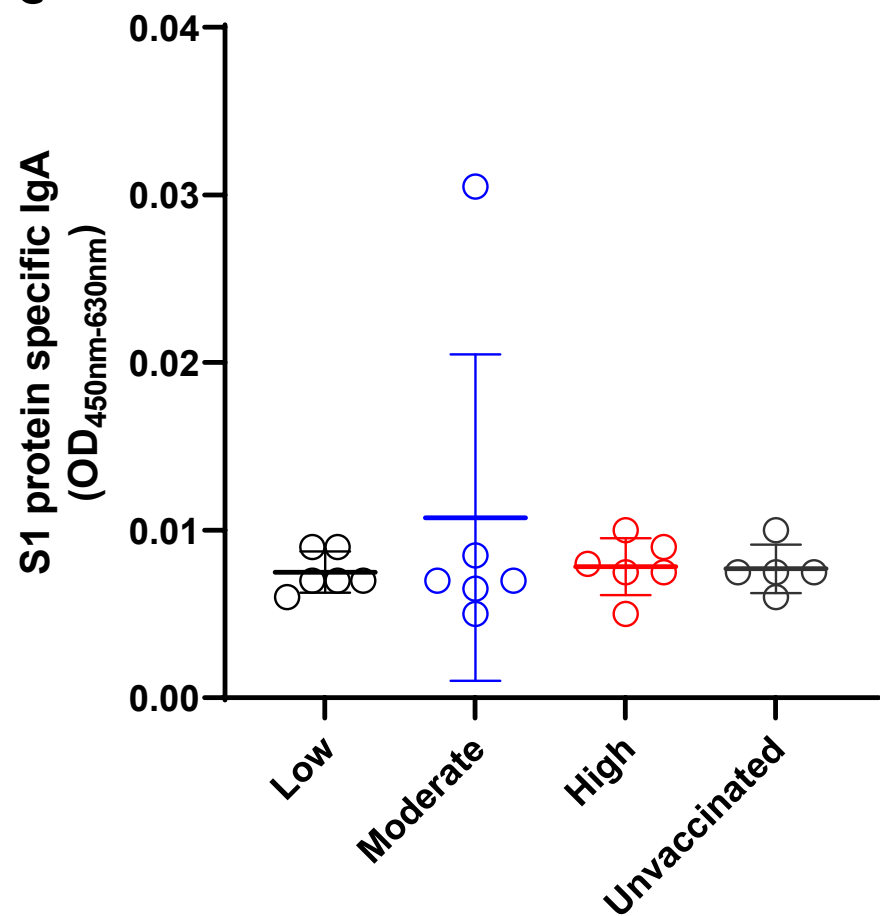
**A**



**B**



**C**



**D**

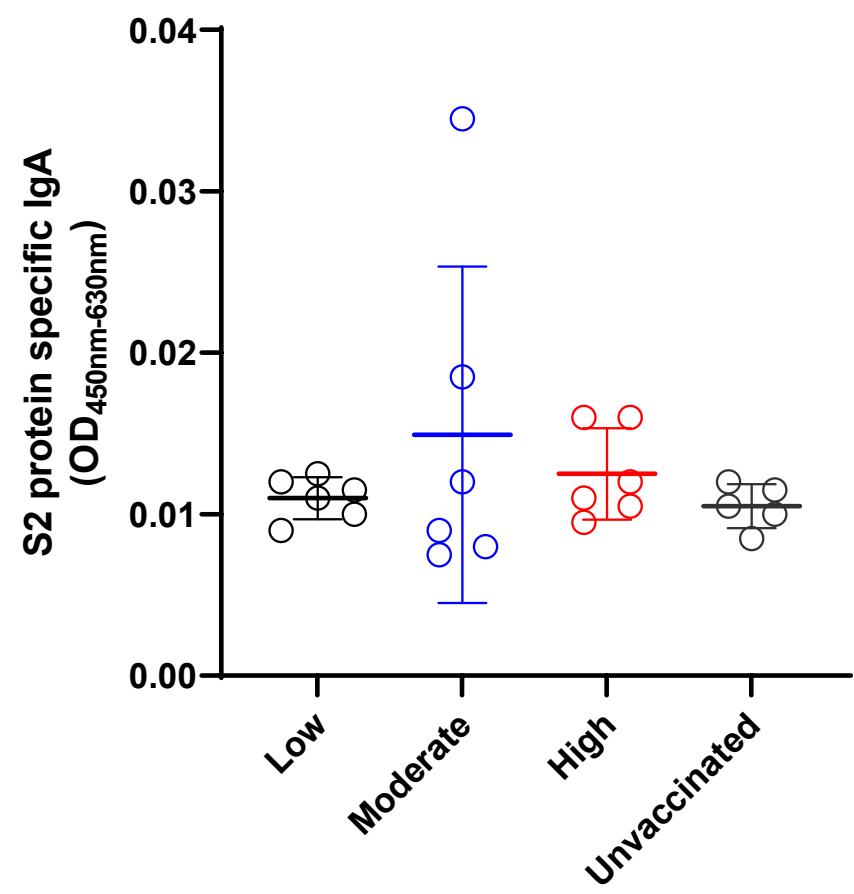




**Figure 8** The impact of pre-existing antibodies on the minimum recognition of epitope P144 after vaccination

medRxiv preprint doi: <https://doi.org/10.1101/2021.07.13.21260404>; this version posted July 15, 2021. The copyright holder for this preprint (which was not certified by peer review) is the author/funder, who has granted medRxiv a license to display the preprint in perpetuity. All rights reserved. No reuse allowed without permission.

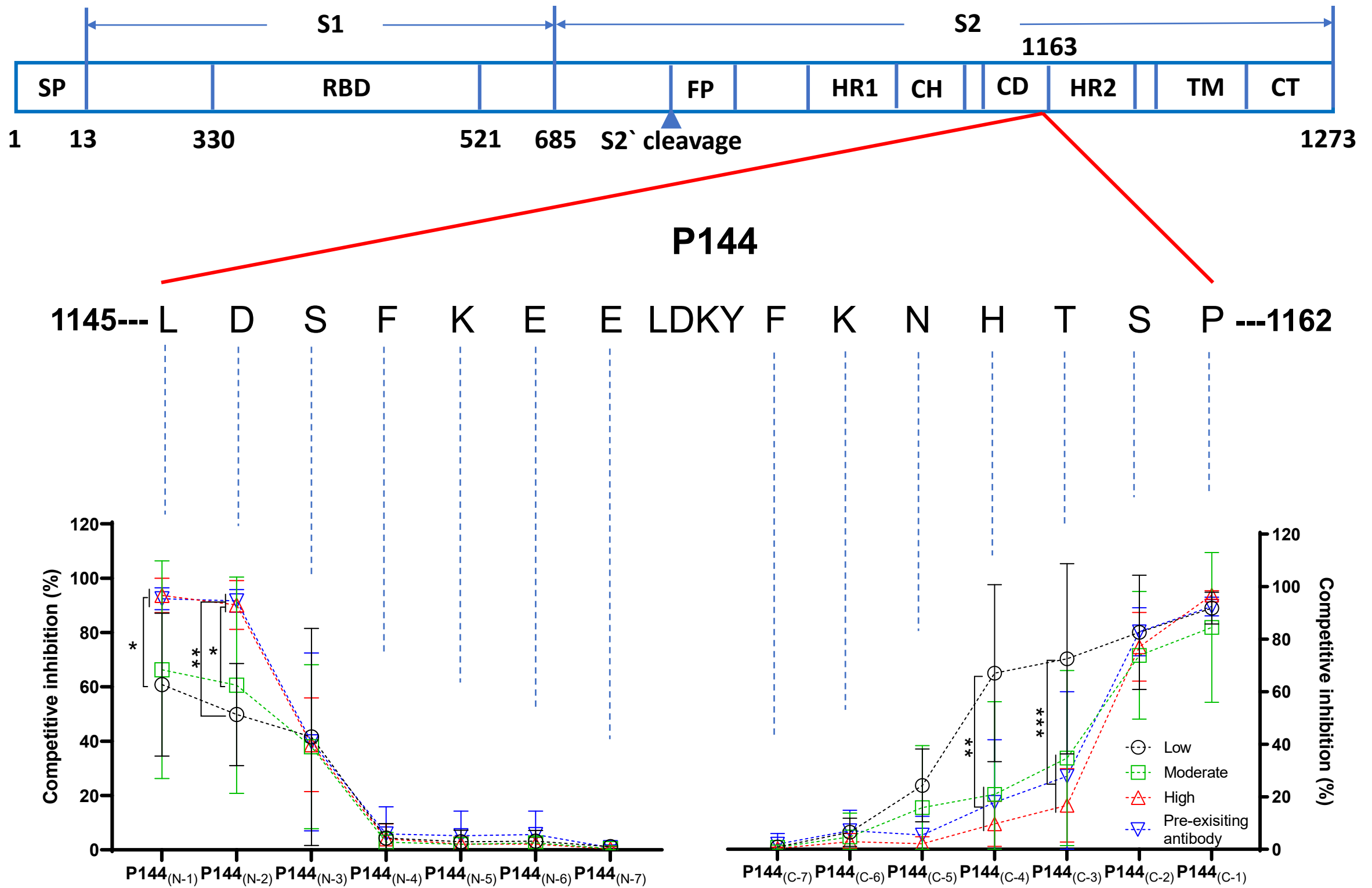


**Figure 9** The impact of pre-existing antibody on the cellular immune responses induced by a DNA vaccine encoding SARS-CoV-2 S protein

**A** medRxiv preprint doi: <https://doi.org/10.1101/2021.07.13.21260404>; this version posted July 15, 2021. The copyright holder for this preprint (which was not certified by peer review) is the author/funder, who has granted medRxiv a license to display the preprint in perpetuity. All rights reserved. No reuse allowed without permission.

